

AD-A088 746

SRI INTERNATIONAL MENLO PARK CA
THEORETICAL STUDY OF STATE-TO-STATE COLLISIONS.(U)
JUN 80 A P HICKMAN, R P SAXON

F/G 20/8

F44620-75-C-0073

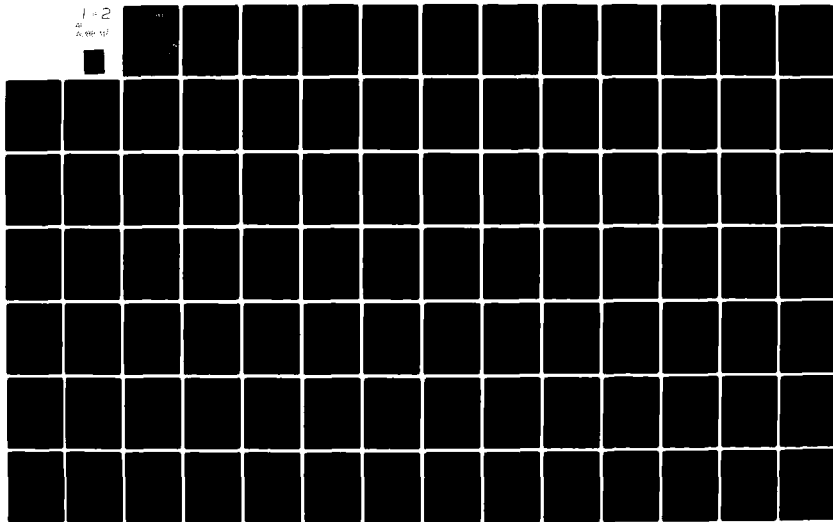
UNCLASSIFIED

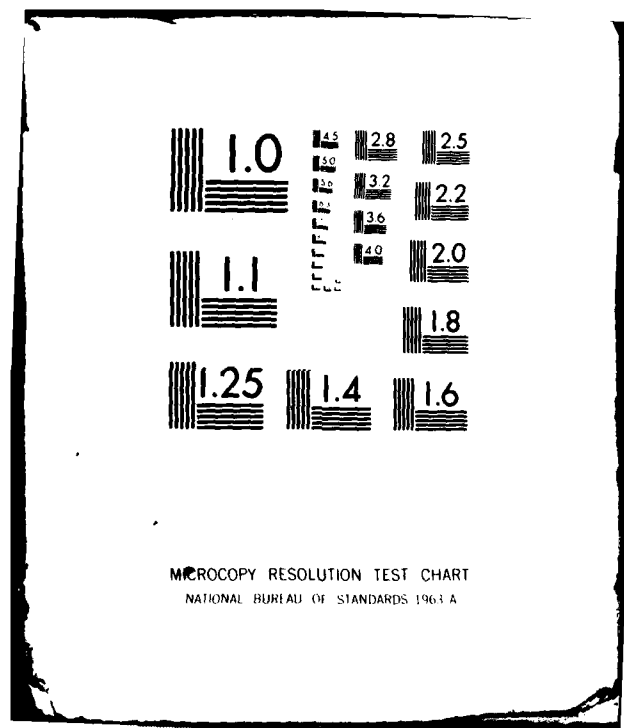
SRI-MP-80-72

AFOSR-TR-80-0682

NL

1 - 2
20
A-088-12





DDC FILE COPY,

AD A088746

SRI International



AFOSR-TR- 80-0682

June 23, 1980

LEVEL II

5

Final Scientific Report
Covering the Period 1 May 1979 to 30 April 1980

THEORETICAL STUDY OF STATE-TO-STATE COLLISIONS

By: Albert P. Hickman and Roberta P. Saxon

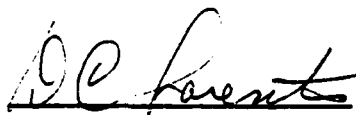
Contract F44620-75-C-0073
SRI Project 4217
MP 80-72

Prepared for:

AIR FORCE OFFICE OF SCIENTIFIC RESEARCH
Bolling Air Force Base
Washington, D.C. 20332

Attention: Dr. Ralph Kelley

Approved:


D. C. Lorents, Director
Molecular Physics Laboratory

P. J. Jorgensen, Vice President
Physical and Life Sciences

DTIC
ELECTED
SEP 4 1980

Approved for public release;
distribution unlimited.

333 Ravenswood Ave. • Menlo Park, California 94025
(415) 326-6200 • Cable: SRI INTL MPK • TWX: 910-373-1246

80 9 2 225

REPORT DOCUMENTATION PAGE		READ INSTRUCTIONS BEFORE COMPLETING FORM
1. REPORT NUMBER (18) AFOSR-TR-30-0682	2. GOVT ACCESSION NO. AD-A088746	3. RECIPIENT'S CATALOG NUMBER
4. TITLE (and Subtitle) (6) Theoretical Study of State-to-State Collisions		5. TYPE OF REPORT & PERIOD COVERED (7) Final Scientific Report 1 May 79 - 30 April 80
7. AUTHOR(s) (10) Albert P. Hickman, Roberta P. Saxon		6. PERFORMING ORG. REPORT NUMBER MP 80-72
9. PERFORMING ORGANIZATION NAME AND ADDRESS SRI International 333 Ravenswood Avenue Menlo Park, California 94025 (11) 23 Jun 80		8. CONTRACT OR GRANT NUMBER(s) (15) F44620-75-C-0073
11. CONTROLLING OFFICE NAME AND ADDRESS Air Force Office of Scientific Research/NP Bolling Air Force Base Washington, D. C. 20332		10. PROGRAM ELEMENT, PROJECT, TASK AREA & WORK UNIT NUMBERS 61102F (16) 2301/A4 (17) A4
14. MONITORING AGENCY NAME & ADDRESS (if different from Controlling Office) (14) SRI-MP-80-72		12. REPORT DATE June 23, 1980
		13. NUMBER OF PAGES 137 (12) 138
		15. SECURITY CLASS. (of this report) Unclassified
		15a. DECLASSIFICATION/DOWNGRADING SCHEDULE
16. DISTRIBUTION STATEMENT (of this Report) Approved for public release; distribution unlimited.		
17. DISTRIBUTION STATEMENT (of the abstract entered in Block 20, if different from Report)		
18. SUPPLEMENTARY NOTES		
19. KEY WORDS (Continue on reverse side if necessary and identify by block number) triatomic collisions, Rydberg atom collisions, potential curves of small molecules, photodissociation, CH ⁺ , nonadiabatic collisions		
20. ABSTRACT (Continue on reverse side if necessary and identify by block number) The probability of making transitions between specifically known molecular states by collision processes has been theoretically investigated. The following research areas have been studied: Collisions of Rydberg states of Na, Rb, and Xe with rare gas atoms and with molecules; calculations of potential curves, matrix elements, and photodissociation cross sections of CH ⁺ , and nonadiabatic collision processes between alkali atoms or rare gas metastables and diatomic molecules that lead to ion-pair formation.		

CONTENTS

Accession For	STIS	GAH	DDC TAB	Unannounced	Justification	By	Distribution/	Availabilty Codes	Avail and/or special	Dist
										A

I	INTRODUCTION	2
II	RESEARCH ACCOMPLISHMENTS	4
	Theoretical Studies of Rydberg Atoms	4
	Theoretical Calculations of Small Molecules: CH^+	6
	Theory of Nonadiabatic Collisions	7
	List of Papers Completed, 1975-80	15
III	REFERENCES	18
	APPENDICES	
	A. Approximate Scaling Formula for Angular Momentum Changing Collisions of Rydberg Atoms	
	B. Excited States of CH^+ Potential Curves and Transition Moments	
	C. Comparison of Ion-Pair Formation in the Systems $AR^* + I_2$ and $K + I_2$	
	D. Model for Fast, Nonadiabatic Collisions between Alkali Atoms and Diatomic Molecules	

AIR FORCE OFFICE OF SCIENTIFIC RESEARCH (AFSC)
 NOTICE OF TRANSMITTAL TO DDC
 This technical report has been reviewed and is
 approved for public release IAW AFR 190-12 (7b).
 Distribution is unlimited.
 A. D. BLOSE
 Technical Information Officer

I INTRODUCTION

This is the final report of a project devoted to the theoretical study of molecular state-to-state collision phenomena. The present document describes the work accomplished during the fifth year of the program (1 May 1979 to 30 April 1980). Interim scientific reports dated June 22, 1979, July 1, 1978, June 24, 1977, and June 28, 1976 have covered the work of preceding years.

The purpose of the project has been to develop the theoretical tools necessary to treat a variety of collision processes, and to perform calculations of transition probabilities for selected systems. The problems considered have involved the interactions of three particles under the influence of potentials for two or more electronic states. For this type of process, currently available experimental techniques allow the determination of specific states of species before and after interaction. Our general method of approach has been to pursue two types of calculations: model calculations designed to isolate and probe particular reaction mechanisms, and detailed calculations on specific systems that have been studied experimentally in our laboratory or elsewhere. This dual approach has enabled us better to understand a wide range of scattering phenomena, and has provided a quantitative test of the accuracy of the methods we have developed.

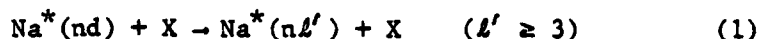
During the past year we have worked on the following types of problems: theoretical studies of collisional angular momentum mixing of highly excited, Rydberg atoms; calculations of potential surfaces, matrix elements, and photodissociation cross sections for small molecules; and the development of new methods to treat the nonadiabatic

process of ion-pair formation in collisions of alkali atoms or rare gas metastables with diatomic molecules. Our accomplishments in these areas are summarized in the following section.

II RESEARCH ACCOMPLISHMENTS

Theoretical Studies of Rydberg Atoms

Studies investigating the properties of highly excited Rydberg atoms have been under way at SRI for several years. The experiments of Gallagher, Edelstein, and Hill¹ first identified the "angular momentum mixing" process:



in 1975. The cross sections for this process are very large and show a maximum when plotted as a function of principal quantum number n . Over a period of years, studies supported by this contract²⁻⁵ have contributed to increased understanding of Rydberg collision processes. The work completed in the past year has furthered this understanding by consolidating the results of several previous calculations in terms of general scaling formulas. These formulas lead to an appealing physical interpretation of the process of angular momentum mixing, and can be quickly and easily applied to a variety of systems.

During the past year, in work supported by another Air Force contract, the research group of T. F. Gallagher has studied collisions of Na Rydberg atoms with molecules such as CH_4 and C_3H_8 (methane and propane).⁶ The research sought to determine the role of the internal structure of the collision partner. The experimental data obtained was qualitatively very similar to data obtained for much simpler collision partners, such as the rare gases He, Ne, and Ar,¹ and also for N_2 .⁵ These results suggested that the larger and more complicated collision partners could be treated by the same theoretical model^{4,5} that was successfully used to analyze collisions with structureless particles. The only information required for this model is data for low energy electron scattering from CH_4 and C_3H_8 , which is available.

Because of the apparent wide range of validity of the theoretical model we have used, and because of the small number of parameters on which the results depend, we sought to express the results in terms of physical scaling laws. We have found that the results of many coupled-channel and Born calculations can be expressed in terms of numerically determined functions of reduced parameters. The general result is

$$\sigma_{l\text{-mix}}(n) = \pi n^4 a_0^2 g(\beta) f(\gamma) \quad (2)$$

where $\sigma_{l\text{-mix}}(n)$ is the experimentally measured cross section for process (1), summed over all final states l' ; β is a quantity that measures the strength of the interaction of the collision partner with the diffuse electron cloud; and γ is a quantity related to the energy gap between the nd and higher nl states of Na. Equation (2) thus leads to an interpretation of the scattering process in terms of reduced parameters that have a clear physical meaning. The formula has been applied to collisions of Na(nd) with He, Ne, Ar, N_2 , CH_4 , C_3H_8 ; to Rb(nf) + He, Ar, Xe; and to Xe(nf) + CO_2 . The results are generally accurate to about a factor of two. This degree of accuracy is very useful because the cross sections vary by an order of magnitude or more in the range of n considered. This work has been submitted to Physical Review A, and a preprint is included as Appendix A. This preprint contains a more complete discussion of the scaling formula, as well as graphs of the functions $f(\gamma)$ and $g(\beta)$ of Eq. (2).

The most important theoretical result of our work on Rydberg atoms has been to achieve a better understanding of the role of the interaction of the excited electron with the collision partner. It had generally been argued that the interaction of a Rydberg atoms with a collision partner should be determined by the way the excited electron, in its large orbit, scattered from the collision partner. The quantitative calculations we have done lend support to this physical picture, and explain the mechanism in much greater detail.

Theoretical Calculations of Small Molecules: CH⁺

The formation and destruction of CH⁺ in diffuse interstellar clouds is an interesting problem in interstellar chemistry. Better knowledge of the excited state potential curves as well as of photodissociation cross sections is necessary to understand this astrophysical problem. The CH⁺ system is small enough so that calculations that include Rydberg states on the same footing as valence states could be undertaken. In collaboration with Dr. Bowen Liu, IBM Research Laboratory, San Jose, CA, and Dr. Kate Kirby, Harvard-Smithsonian Center for Astrophysics, Cambridge, MA, we performed ab initio calculations of the valence and low-lying Rydberg states of ¹Π and ¹Σ symmetry of CH⁺. The specific objective of this work was to explore the repulsive excited states of CH⁺ as well as to look for bound excited states that are dipole-connected to the ground X¹Σ⁺ state to investigate whether CH⁺ is a source for unidentified interstellar molecular absorption lines. Only the first root of each symmetry is bound, although the 2¹Σ⁺ state is found to be quasi-bound in this calculation. Transition moments and photodissociation cross sections from the X¹Σ⁺ state to a number of excited ¹Σ⁺ and ¹Π states were calculated; it was found that the 3¹Σ⁺ and 2¹Π states have significant cross sections at wavelengths longer than Lyman-α. From these cross sections and astrophysical information, photodissociation rates in interstellar clouds and comets can be obtained.

Photodissociation cross sections and their astrophysical implications are discussed in a paper accepted by the Astrophysical Journal.⁷ The ab initio calculations, in which care was taken to test the validity of the calculational procedure, are described in a paper that has been accepted by the Journal of Chemical Physics. A preprint of the latter paper is attached as Appendix B.

We have also recently completed a calculation of the $^3\Sigma^-$ state of CH^+ which correlates asymptotically to $\text{C}(^3\text{P}) + \text{H}^+$. This system is being studied experimentally in the Molecular Physics Laboratory by the technique of fast beam photofragment spectroscopy. Knowledge of the $^3\Sigma^-$ potential curve may aid in interpreting the experimental data. This particular state of CH^+ poses an interesting theoretical challenge as well. While there is no electron on the H^+ , asymptotically there is H character in the molecular orbitals in the bonding region. Thus, designing a calculation to determine properly the molecular orbitals requires some care. We have carried out a series of calculations including different amounts of electronic correlation and have compared the results in terms of the spectroscopic parameters describing the minimum and maximum of the potential curve. The excellent agreement between the different calculations confirms that we have realistically described the $\text{CH}^+ ^3\Sigma^-$ potential curve.

Theory of Nonadiabatic Collisions

During the past year we made substantial progress in the study of atom-molecule collisions that involve two or more electronic potential energy surfaces. Although the approaches we developed are applicable to many different systems, we generally focused on systems that were actively being investigated in the experimental program at SRI.

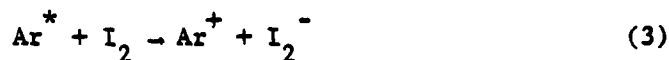
We have used three types of theoretical approaches. The first is a quasi-classical trajectory model that invokes the Landau-Zener formula to calculate a "surface-hopping" probability at each surface intersection. Such a model has yielded reasonable results for many systems,⁸⁻¹¹ but its quantitative accuracy may be limited in certain situations, such as the reaction of $\text{He}(2^{1,3}\text{S})$ with O_2 now being studied at SRI -- a reaction that involves three surfaces. Therefore, we have

also pursued two different quantum mechanical approaches. One of these is based on applying time-dependent perturbation theory in the impact parameter formulation. We assume the projectile follows a straight line, constant velocity classical trajectory of a given impact parameter. The potential seen by the target diatomic molecule is then explicitly time-dependent. The other quantum mechanical approach, which is time-independent, is a generalization of the quantum mechanical Infinite-Order-Sudden (IOS) approximation.^{12,13} This method has been extensively applied to rotational excitation.^{12,14} In this approximation, the solution of the coupled equations is greatly simplified, when one assumes the rotational levels for a given vibrational state are degenerate, and solves coupled channel equations for only the number of vibrational states of interest. We have found that similar expressions can be derived when several electronic states are coupled. They can be made extremely simple if one assumes that both the rotational and vibrational levels are degenerate. Although this approximation must be tested further, it looks promising at the experimental energies of interest. The following subsections discuss our results with each of these three approaches.

(a) Quasi-Classical Surface Hopping Model

The work done in this area was an outgrowth of a collaboration with Dr. Aart Kleyn of the FOM institute in Amsterdam. Kleyn visited SRI for two months in 1979 and implemented some of the computer codes used in Amsterdam. We have done additional work to modify and generalize these codes.

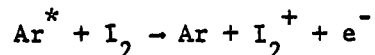
Using the surface-hopping model, we performed a comparative study of ion-pair formation on two similar systems:



and



One would expect these two reactions to be rather similar, since in each case the single active electron is in a 4s orbital. However, an additional final channel is available in the first reaction. Penning ionization may occur,



Data are available for both reactions. The FOM group in Amsterdam considered $K + I_2$ ^{10,11} and Dr. K. T. Gillen at SRI has investigated $Ar^* + I_2$. In a collaborative effort with Dr. Gillen, we were able to perform calculations that explained some of the differences in the differential cross sections for these two systems. We explored how differences in the matrix elements arising from the inner shell vacancy and the competing ionization channel would affect the cross sections. This work has been submitted to the Journal of Chemical Physics, and a preprint is included as Appendix C.

(b) Quantum Mechanical Perturbation Theory of Nonadiabatic Collisions

Considerable theoretical effort¹⁵ has been directed to the quantum mechanical formulation of the nonadiabatic (i.e., multiple-potential-surface) collision problem. The most general theory, and the least tractable, is a full coupled-channel expansion in rotational, vibrational, and electronic eigenstates. We sought an alternative formulation that preserved the essential features of the multiple-surface crossings, but exploited approximations that can legitimately be made at the high collision energies of interest ($E \sim 50-100$ eV). The approach chosen was the impact parameter approximation,¹⁶ in which a rectilinear classical trajectory is assumed for the translational motion, leading to a time-dependent Schroedinger's equation for the

remaining degrees of freedom. We discovered that model potentials of the same type used in previous studies of collisions of alkali atoms and diatomic molecules led to a particularly simple form of the final equations. These equations were solved using the Magnus approximation.¹⁷

We will briefly summarize the results of our calculations. We performed calculations using model potentials chosen to model the reaction



Initially, isotropic potentials were assumed; that is, molecular rotation was neglected. The results exhibited strong oscillations, corresponding qualitatively to those observed in recent measurements.¹⁸ These oscillations have been related to the vibrational motion of the molecular O_2 or O_2^- during the time of the collision. We also treated anisotropic potentials using the Infinite-Order-Sudden approximation. We obtained rotationally averaged cross sections between specific vibrational states. The oscillations observed in the isotropic case persisted, although they were less prominent.

These rotationally averaged calculations also enabled us to examine the effect of different initial vibrational levels v_1 on the ion pair formation. The model predicted that the oscillations will become less pronounced as v_1 is increased. Although no measurements are available to test this result, our calculations suggest a direction for future experiments.

The theory and calculations are described in greater detail in a paper that has been submitted to the Journal of Chemical Physics. A preprint is included as Appendix D.

(c) Time-Independent Quantum Mechanical Theory of Nonadiabatic Collisions

The time-independent theory of nonadiabatic collisions that we are developing is a generalization of the usual IOS approximation and is complementary to the impact parameter approach described above. The impact parameter treatment assumes a straight line trajectory, but explicitly considers the internal state structure, whereas methods based on the sudden approximation properly treat the dynamics, but assume internal energies are degenerate.

The sudden approximation is conceptually appealing for our application to systems like $\text{He}^* + \text{O}_2$, since in the experiments rotational states of the target are not resolved and in the sudden approximation they do not have to be considered individually. Although the IOS formalism has been given^{12,13} for the case where vibrational channels are considered explicitly, most calculations have been done in the rigid rotor approximation (i.e., ignoring vibration).

In the present work, we develop the time-independent close coupled equations for the case of two electronic states in the sudden approximation for all internal degrees of freedom, that is, vibrational and rotational. We start with a Hamiltonian expressed in terms of the matrix elements between the electronic eigenstates. We then seek a solution to the time-independent Schroedinger equation. The solution is written as the column vector $\begin{bmatrix} \psi_0(R,r) \\ \psi_1(R,r) \end{bmatrix}$, where the wavefunctions on the covalent and ionic surfaces, respectively, are given by expansions in terms of the internal states of O_2 and O_2^- .

$$\psi_0(R,r) = \sum_i F_i(R) \phi_i(r) \quad (7)$$

$$\psi_1(R,r) = \sum_i G_i(R) \chi_i(r) \quad (8)$$

In this case $\phi_i(r)$ and $\chi_j(r)$ refer to all internal degrees of freedom; that is, r refers to all internal coordinates. In the sudden approximation, we solve the simplified set of two coupled equations:

$$\left[\frac{d^2}{dR^2} - \frac{\bar{l}(\bar{l}+1)}{R^2} + \bar{k}^{-2} \right] \begin{pmatrix} f(R,r) \\ g(R,r) \end{pmatrix} - \frac{2\mu}{\hbar^2} \begin{bmatrix} V_{00}(R,r) & V_{01}(R,r) \\ V_{01}(R,r) & V_{11}(R,r) \end{bmatrix} \begin{bmatrix} f(R,r) \\ g(R,r) \end{bmatrix} = 0 \quad (9)$$

Here \bar{l} is an appropriately chosen value of the orbital angular momentum and $\bar{k}^2 = \frac{2\mu}{\hbar^2} (E - \bar{\epsilon})$, where $\bar{\epsilon}$ is an average internal energy for the two electronic states, for the functions $f(R,r)$ and $g(R,r)$. Replacing l by \bar{l} and the internal energies by an average value are the heart of the sudden approximation. In Eq. (9), the internal coordinates denoted by r are considered as fixed parameters. The desired solutions of the original problem are then given as:

$$F_{in}(R) = \langle \phi_i(r) | f(R,r) | \phi_n(r) \rangle \quad (10)$$

$$G_{jn}(R) = \langle \chi_j(r) | g(R,r) | \phi_n(r) \rangle \quad (11)$$

Roughly speaking, Eqs. (10) and (11) average the solutions $f(R,r)$ and $g(R,r)$ for fixed values of r over the internal wavefunctions in r . In the present formulation, the number of coupled equations is just the number of electronic surfaces in the problem.

The S matrix elements are written on terms of four $N \times N$ blocks whose elements are S_{ij}^{00} , S_{ij}^{01} , S_{ij}^{10} , and S_{ij}^{11} , where the superscripts denote the initial and final electronic surface, and the subscripts denote the initial and final target state. In terms of the 2×2 S matrix calculated by solving Eq. (9), whose elements are S_{00} , S_{01} , S_{11} , we have

$$S_{ij}^{00} = \langle \varphi_i(r) | S_{00} | \varphi_j(r) \rangle \quad (12)$$

$$S_{ij}^{01} = \langle \varphi_i(r) | S_{01} | \chi_j(r) \rangle \quad (13)$$

$$S_{ij}^{10} = \langle \chi_i(r) | S_{10} | \varphi_j(r) \rangle \quad (14)$$

$$S_{ij}^{11} = \langle \chi_i(r) | S_{11} | \chi_j(r) \rangle \quad (15)$$

In this work we are interested in the total cross section for scattering from a particular vibrational state i on one electronic surface to vibrational state j on the other electronic potential surface, where the cross section has been summed over all final rotational states. We now note that the internal coordinate stands for the vibrational coordinate as well as the body fixed angle, γ , between the diatomic axis and the vector from the diatomic center of mass to the third body. Then the desired cross section is

$$\sigma_{10}(j \leftarrow i) = \frac{1}{2} \int_{-1}^1 \sigma_{10}(j \leftarrow i; \gamma) d \cos \gamma \quad (16)$$

where

$$\sigma_{10}(j \leftarrow i; \gamma) = \frac{\pi}{k^2} \sum_{\bar{l}} (2\bar{l} + 1) |S_{ij}^{10}(\bar{l}, \gamma)|^2 \quad (17)$$

Here we have explicitly written the dependence of S_{ij}^{10} on the angular momentum \bar{l} and angle γ .

For our first application of this formalism, we used the following model potential functions:

$$V_{00}(R) = C_1 \exp(-C_2 R) \quad (18)$$

$$V_{11}(R) = V_{00}(R) - 1/R + \Delta E \quad (19)$$

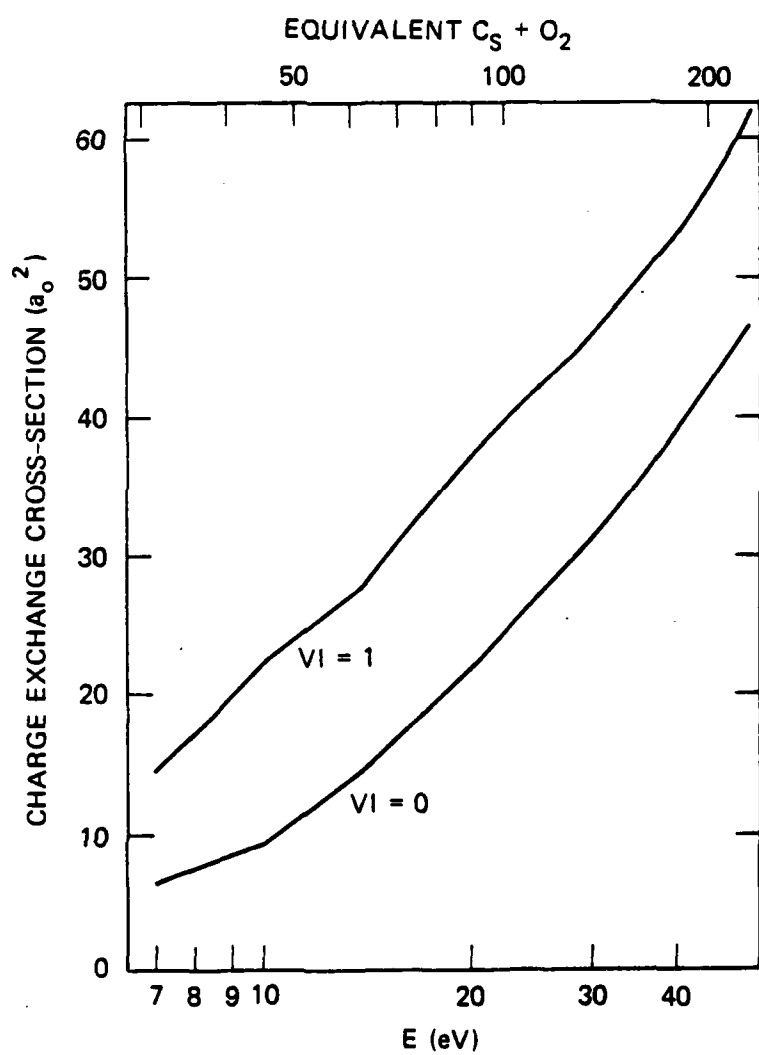
$$V_{01}(R) = C_3 \exp(-C_4 R) \sin 2\gamma \quad (20)$$

where ΔE is the asymptotic separation between the electronic states. The parameters $C_1 = 319.8680$ a.u., $C_2 = 1.9319$ a.u., $C_3 = 0.35$ a.u., $C_4 = 0.5$ a.u., and $\Delta E = 0.12578$ a.u., were chosen to model the reaction



The calculations now completed have assumed that $\sin 2\gamma$ is fixed at 1.0. The cross sections were summed explicitly over final vibrational states. Calculations were performed for a system with the reduced mass of $\text{Li} + \text{O}_2$ to reduce the amount of computation required. The internal energy $\bar{\epsilon}_0$ was taken as the vibrational energy of state i of O_2 , and the internal energy of $\bar{\epsilon}$ was taken as the internal energy of state j of O_2^- .

Results are shown in Fig. 1 for initial vibrational states 0 and 1. The energy scale on the top of the figure also shows the total energy for the $\text{Cs} + \text{O}_2$ system with the same relative velocity as that of the $\text{Li} + \text{O}_2$ mass. Calculations must be performed at higher total energies before the results can be evaluated. The increase of the cross section with initial vibrational state is also apparent in the figure. Future work also includes study of the effect of the choice of $\bar{\epsilon}$ on the results and the evaluation of the charge exchange cross section for anisotropic potentials.



SA-4217-56

Figure 1. Preliminary results of calculations based on the Infinite-Order-Sudden approximation.

List of Papers Completed, 1975-1980

1. F. T. Smith, D. L. Huestis, D. Mukherjee, and W. H. Miller, "Semiclassical Perturbation Scattering by a Rigid Dipole," Phys. Rev. Lett. 35, 1073 (1975).
2. T. F. Gallagher, R. E. Olson, S. A. Edelstein, and R. M. Hill, "Collisional Angular Momentum Mixing of Highly Excited Na (n^2D) by N_2 and CO," Phys. Rev. A 16, 441 (1977).
3. R. E. Olson, "Theoretical Excitation Transfer Cross Sections for Rydberg Na ($n^2D - n^2F$) Transitions from Collisions with He, Ne, Ar," Phys. Rev. A 15, 631 (1977).
4. A. P. Hickman and H. Morgner, "Calculation of Associative and Penning Ionization of H and D by He (2^1S) and He (2^3S)," J. Chem. Phys. 67, 5484 (1977).
5. R. P. Saxon, R. E. Olson, and B. Liu, "Ab Initio Calculations for the $X^2\Sigma$, $A^2\Pi$, $B^2\Sigma$ States of Na Ar: Emission Spectra and Cross Sections for Fine-Structure Transitions in Na-Ar Collisions," J. Chem. Phys. 67, 2692 (1977).
6. W. H. Miller and F. T. Smith, "Semiclassical Perturbation Theory of Electron-Molecule Collisions," Phys. Rev. A 17, 939 (1978).
7. D. Mukherjee and F. T. Smith, "Semiclassical Perturbation Scattering Theory of Electron-Polar Molecule Collisions: Total Excitation and Scattering Cross Sections," Phys. Rev. A 17, 954 (1978).
8. A. P. Hickman and F. T. Smith, "Momentum Transfer in Electron-Polar Molecule Collisions: Results of Semiclassical Perturbation Scattering Theory," Phys. Rev. A 17, 969 (1978).
9. B. Liu and R. E. Olson, "Potential Energies for Ca_2^+ : Cross Sections for Collisions of Ca^+ and Rydberg Ca^{**} with Ca," Phys. Rev. A 18, 2498 (1978).
10. R. P. Saxon, K. Kirby, and B. Liu, "Ab Initio Configuration Interaction Study of The Low-Lying Electronic States of MgH," J. Chem. Phys. 69, 5301 (1978).
11. A. P. Hickman, "Theory of Angular Momentum Mixing in Rydberg Atom-Rare Gas Collisions," Phys. Rev. A 18, 1339 (1978).

12. A. P. Hickman, "Relation Between Low-energy Electron Scattering and λ -Changing Collisions of Rydberg Atoms," Phys. Rev. A 19, 994 (1979).
13. R. E. Olson, "Rydberg Atom-Rydberg Atom Ionization Cross Sections," J. Phys. B 12, L109 (1979).
14. K. Kirby, R. P. Saxon, and B. Liu, "Oscillator Strengths and Photodissociation Cross Sections in the $\chi \rightarrow A$ and $\chi \rightarrow B$ Band Systems in MgH; Astrophys. J. 231, 637 (1979).
15. K. Kirby, W. Roberge, R. P. Saxon, and B. Liu, "Photodissociation Cross Sections and Rates for CH^+ in Interstellar Clouds," Astrophys. J., in press.
16. K. Kirby, R. P. Saxon, and B. Liu, "Excited States of CH^+ : Potential Curves and Transition Moments," J. Chem. Phys., in press.
17. A. P. Hickman, "Approximate Scaling Formula for Angular Momentum Changing Collisions of Rydberg Atoms," submitted to Phys. Rev. A.
18. A. P. Hickman and K. T. Gillen, "Comparison of Ion-Pair Formation in the Systems $Ar^* + I_2$ and $K + I_2$," submitted to J. Chem. Phys.
19. A. P. Hickman, "Model for Fast, Nonadiabatic Collisions Between Alkali Atoms and Diatomic Molecules," submitted to J. Chem. Phys.

III REFERENCES

1. T. F. Gallagher, S. A. Edelstein, and R. M. Hill, Phys. Rev. Lett. 35, 654 (1975); Phys. Rev. A 15, 1945 (1977).
2. R. E. Olson, Phys. Rev. A 15, 631 (1977).
3. A. P. Hickman, Phys. Rev. A 18, 1339 (1978).
4. A. P. Hickman, Phys. Rev. A 19, 994 (1979).
5. T. F. Gallagher, R. E. Olson, W. E. Cooke, S. A. Edelstein, and R. M. Hill, Phys. Rev. A 16, 441 (1977).
6. K. A. Safinya and T. F. Gallagher, Phys. Rev. A., in press.
7. K. Kirby, W. Roberge, R. P. Saxon, and B. Liu, Astrophys J., in press.
8. F. Biraben, Thèse, Paris VI (1977).
9. A. W. Kleyn, M. M. Hubers, and J. Los, Chem. Phys. 34, 55 (1978).
10. J. A. Aten, G.E.H. Lanting, and J. Los, Chem. Phys. 19, 241 (1977).
11. J. A. Aten and J. A. Los, Chem. Phys. 25, 47 (1977).
12. G. A. Parker and R. T. Pack, J. Chem. Phys. 68, 1585 (1978).
13. D. Secrest, J. Chem. Phys. 62, 710 (1975).
14. D. J. Kouri, in Atom-Molecule Collision Theory, R. B. Bernstein, ed. (Plenum, NY, 1979).
15. For example, see review by M. S. Child, in Atomic-Molecule Collision Theory, R. B. Bernstein, ed. (Plenum, NY, 1979).
16. S. Geltman, Topics in Atomic Collision Theory (Academic Press, NY, 1969).
17. P. Pechukas and J. C. Light, J. Chem. Phys. 44, 3897 (1966).
18. A. W. Kleyn, M. M. Hubers, and J. Los, Chem. Phys. 34, 55 (1978).

APPENDIX A

APPROXIMATE SCALING FORMULA FOR COLLISIONAL ANGULAR MOMENTUM MIXING OF RYDBERG ATOMS

A. P. Hickman
Molecular Physics Laboratory
SRI International, Menlo Park, CA 94025

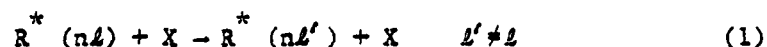
ABSTRACT

An approximate scaling formula has been determined that permits the rapid estimation of cross sections for angular momentum changing collisions of Rydberg atoms with a variety of targets, using information about low energy electron scattering from the target. The formula is obtained by fitting the results of coupled-channel and Born approximation calculations to functions of reduced parameters. Application to $\text{Na(nd)} + \text{He, Ne, Ar, N}_2, \text{CH}_4, \text{C}_3\text{H}_8$; $\text{Rb(nf)} + \text{He, Ar, Xe}$; and $\text{Xe(nf)} + \text{CO}_2$, suggests that the accuracy is about a factor of two.

MP 80-73

I INTRODUCTION

Considerable attention has been devoted recently to collisions involving Rydberg atoms, especially the " ℓ -mixing" or angular momentum changing process¹⁻¹¹



where R^* is the Rydberg atom and X is the collision partner. It has generally been argued that one should be able to analyze this process in terms of the cross section for low energy electron scattering from X . In this paper we present a very simple scaling formula that can be used to estimate the cross section for reaction (1) to about a factor of two, starting from information about e - X scattering. This degree of accuracy is useful because the cross sections may vary by as much as an order of magnitude over the range of n considered.

The scaling formula was determined by fitting the results of coupled-channel and Born approximation calculations to functions of reduced parameters. These parameters have a reasonable physical interpretation in terms of the "nearly free electron" picture. The determination of the formula and its physical interpretation are discussed in Section II. Section III contains the results of calculations for several systems, including molecular targets. The accuracy of the results for more complicated targets suggests that their internal structure may play only a minor role in the collisions studied.

II THE SCALING FORMULA

A. Determination

Our previous calculations^{6,8} of angular momentum mixing may be characterized as exact or approximate solutions of a specific, well-defined model problem. We will begin by summarizing this problem, and then show how one might expect to estimate the desired cross sections using empirical functions of reduced parameters. Then one additional approximation is introduced to tie the model problem to the physical system involving the Rydberg atom and an arbitrary collision partner.

The model problem may be posed as follows. Consider the system $\text{Na}^* + \text{X}$ indicated in Figure 1. The Rydberg atom Na^* has principle quantum number n , and we consider only the initial level $l=2$ and other levels $l=3,4,\dots,n-1$. Assume

$$E_{nl} - E_{nd} = \Delta E, \quad l=3,4,\dots,n-1 \quad (2)$$

This is approximately true for sodium since the d quantum defect δ_d is much larger than δ_l for $l > 2$. The interaction potential is given by a Fermi pseudopotential

$$V(\vec{R}, \vec{r}) = 2\pi A \delta(\vec{r} - \vec{R}) \quad (3)$$

For the present discussion, A is to be considered an arbitrary constant.

We wish to calculate $\sigma_{l\text{-mix}}$, defined by

$$\sigma_{l\text{-mix}} = \sum_{l=3}^{n-1} \sigma(nd - nl), \quad (4)$$

using the quantum mechanical Arthurs and Dalgarno¹³ formalism or the Born approximation as discussed previously.^{6,8} We expect that $\sigma_{L\text{-mix}}$ will depend on n , A , ΔE , and v , the relative velocity of Na^+ and X . That is,

$$\sigma_{L\text{-mix}} = \sigma_{L\text{-mix}}(n, A, \Delta E, v) \quad (5)$$

We wish to find a functional form for $\sigma_{L\text{-mix}}$. Previously, we showed⁸ that if $\Delta E = 0$, the results of the Born approximation may be well-fitted by

$$\sigma_{L\text{-mix}} \propto \left(\frac{A}{v}\right)^2 n^{-2.733} \quad (\Delta E=0) \quad (6)$$

We can write this in a slightly different form by separating out a factor $\pi n^4 a_0^2$ (the so-called geometrical cross section of the Rydberg atom), and making A/v dimensionless by dividing by the unit length and velocity in atomic units:

$$\sigma_{L\text{-mix}} \propto \pi n^4 a_0^2 \beta^2 \quad (\Delta E=0) \quad (7)$$

where

$$\beta^2 = \frac{A^2}{\pi_e^2 a_0^4} \frac{1}{v^2 n^{2.733}} \quad (8)$$

The constant π_e is the electron mass in atomic units. If $\Delta E \neq 0$ our previous results⁸ suggested that in the weak coupling limit a more general formula could be written

$$\sigma_{L\text{-mix}} \propto \pi n^4 a_0^2 \beta^2 f(v) \quad (9)$$

where

$$\gamma = \frac{n^2 a_0^2 \Delta E}{\hbar v} \quad (10)$$

$f(\gamma)$ is an approximation to the family of functions shown in Figure 2 of reference 8 that depend weakly on the parameter n . In neglecting the dependence on n we simplify the functional form but introduce some ambiguity into the determination of f . Eq. (9) is expected to be a reasonable approximation in the weak-coupling (small A or large n) limit. We now postulate that a more general formula can be obtained by writing

$$\sigma_{2\text{-mix}} = \pi n^4 a_0^2 g(\beta) f(\gamma) \quad (11)$$

where

$$g(\beta) \rightarrow \lambda \beta^2 \text{ as } \beta \rightarrow 0 \quad (12)$$

We will find later the constant γ has the value 0.715. We performed a number of calculations using the coupled channel method and Born approximation to test the usefulness of Eq. (11). For the situations previously considered, the Born approximation could be applied only when n was large, and the coupled channel method was feasible only when n - and the number of channels - was small. However, by varying A and v , we have been able to probe a wider region of β - γ space and still keep the number of channels small. The results of these calculations are listed in Table 1.

It was possible to find, empirically, functions $f(v)$ and $g(\beta)$ such that the results of the coupled channel and Born approximation calculations were approximated by Eq. (11) to about a factor of two. These functions are shown in Figures 2 and 3 and tabulated in Tables 2 and 3.

At this point we have obtained an approximate scaling rule that can be used to estimate the results of a model problem involving a Fermi pseudopotential with arbitrary constant A . We now make an additional approximation to relate A to the low-energy electron scattering by X . Let

$$4 \pi A^2 = \sigma_{el} (1/2n^2) \quad (13)$$

σ_{el} is the e-X scattering cross section at the electron energy $1/2n^2$, which is the average kinetic energy of the electron in the quantum level n . As $n \rightarrow \infty$, $A \rightarrow L$, the scattering length. Some justification is given for Eq. (13) in reference 8. In this work we find, a posteriori, that it is reasonably successful.

With the substitution defined by Eq. (13), the final form of the scaling rule is given by Eqs. (10), (11), and

$$\beta = \frac{A}{\pi a_0^2} \frac{1}{vn} \left[\frac{\sigma_{el}(1/2n^2)}{4\pi} \right]^{1/2} \quad (14)$$

Although the scaling rule is empirical, it can be related to a natural physical interpretation of the scattering process. This interpretation will be discussed in the next section. Finally, note

that although the preceeding discussion has assumed that the Rydberg atom was sodium, we find that the formula may be applied to other atoms as well. The essential feature of the model is that the initial level is separated by ΔE from a nearly degenerate set of possible final levels. For large n , the difference in the number of final states for an initial $l=2$ or 3 is small. Hence we will test the formula for collisions involving Na (nd), Rb (nf), and Xe (nf).

B. Physical Interpretation and Discussion

The approximate scaling formula is a product of three factors. The geometrical factor $\pi n^4 a_0^2$ shows that the cross section scales with the overall size of the atom. We interpret the parameter β as a coupling strength, and $g(\beta)$ as the probability that the collision partner will encounter the orbiting Rydberg electron. β increases with σ_{el} , which gives an effective size of the collision partner, and decreases with n , because for larger n the electron "cloud" is more diffuse. We interpret the function $f(\gamma)$ as the probability that an elastic collision between the orbiting electron and the collision partner will cause a transition into a new energy level. It is interesting to note that the parameter γ may be rewritten

$$\gamma \approx (\Delta\delta) \frac{v_e}{v} \quad (15)$$

where $\Delta\delta$ is the difference in the quantum defects of initial and final states, and $v_e = 1/n$ (atomic units), the velocity corresponding to the

average kinetic energy of an electron with principle quantum number n .

This formula is obtained by expanding

$$\Delta E = \frac{1}{2(n+\delta_{l'})^2} - \frac{1}{2(n+\delta_l)^2} \quad (16)$$

in the limit $\delta_l \ll n$ and substituting into Eq. (10). When γ is large, $f(\gamma) \rightarrow 0$ and hence the l -mixing will be small. Eq. (15) shows that this can occur because the inelasticity is large, or because v_e is large compared to v , and hence it is less likely that a collision will deflect the electron enough to change the shape of its orbit. Conversely, the l -mixing will be larger when γ is small. This may occur either because the energy difference between initial and final states is small, or because the electron is moving slowly relative to the collision partner and a collision tends seriously to perturb its orbit.

It is instructive to consider various limiting values of the scaling functions g and f . We have already noted that the function g is parabolic as the argument approaches zero. For large values of the argument, g tends to saturate at a value of 0.5 to 0.6. This number is somewhat arbitrary since the prefactor $\pi n^4 a_0^2$ could equally well have been $2\pi n^4 a_0^2$ or $4\pi n^4 a_0^2$. Appropriate limiting values of $f(\gamma)$ are more easily defined. As $\Delta E \rightarrow 0$ (or $v \rightarrow \infty$), $\gamma \rightarrow 0$, $f(\gamma) \rightarrow 1$. We can thus draw the following conclusions about the general behavior of

l -mixing cross sections. For large n , $f \rightarrow 1$, and the angular momentum levels nd and $n\ell'$ ($\ell' \geq 2$) are effectively degenerate. The decrease of $\sigma_{l\text{-mix}}(n)$ with increasing n is due to the reduced coupling strength of the diffuse electron cloud. On the other hand, the (inelastic) cross section tends to be small for small n because of the smaller geometrical cross section and the increased importance of the energy level splitting ΔE .

We now consider how the velocity dependence of the l -mixing cross section is controlled by the functions f and g . At large n , γ will generally be sufficiently small so that $f \approx 1$ for typical (thermal) value of v . (Note that $\Delta E \propto n^{-3}$). Then the behavior of $g(\beta)$ shows that $\sigma_{l\text{-mix}}$ decreases for larger values of v . In the limit $v \rightarrow \infty$, $\sigma_{l\text{-mix}} \propto 1/v^2$ but for smaller values of v the dependence may go as $1/v$ or weaker. The $1/v$ dependence corresponds to the intuitive notion that a slower projectile spends more time passing through the Rydberg atom, and consequently has a higher probability of encountering the electron. The opposite may be true for small n when the coupling is stronger. In this case, $g(\beta)$ may achieve its saturated value of $\sim 0.5-0.6$ for a range of thermal velocities, so that the velocity dependence of $\sigma_{l\text{-mix}}$ will be determined by $f(\gamma)$. Examination of Figure () shows that $\sigma_{l\text{-mix}}$ will then increase with larger values of v , because increasing v has the same effect as decreasing ΔE . Similar behavior has been analyzed theoretically in other inelastic collisions by Olson.¹⁴

III RESULTS AND DISCUSSION

A. General Comments

The approximate scaling formula determined in the previous section has been used to estimate angular momentum changing cross sections for collisions of Na(nd) with He, Ne, Ar, N₂, CH₄, and C₃H₈, for collisions of Rb(nf) + He, Ar, and Xe, and for collisions of Xe(nf) + CO₂. The collision velocities used were the mean thermal velocities at the temperatures of the experiments with which the results are compared. This velocity is given by

$$v = \left(\frac{8kT}{\pi\mu} \right)^{1/2} \quad (17)$$

where k is Boltzmann's constant and μ is the reduced mass of the collision system. For collisions involving Na, we used $T = 430$ K; for Rb, $T = 520$ K, and for Xe, $T = 300$ K.

The electron scattering cross sections were determined as follows. For the rare gases Ne, Ar, and Xe, we used the formulas for the s , p , and higher phase shifts given by O'Malley¹⁵ and computed the total elastic scattering cross section in the standard way. For He, we used at every n the value $A = 1.19a_0$ (the scattering length) as the constant term in the Fermi potential [Eq. (3)]. For N₂, following Gallagher et al.,³ we used $A = 0.7a_0$ at every n . For low energy electron scattering ($E \leq 0.5$ eV)

from He and N₂ there is not a strong energy dependence of the cross section. For e-CO₂ and e-CH₄, we used the scattering data compiled by Itikawa.¹⁶ These data are the total momentum transfer cross section, which may include inelastic processes, rather than the elastic cross sections required by the theory. For the CH₄ data, Itikawa estimates an uncertainty in the data of about a factor of two. At this level of accuracy, and at the very low electron energies involved, the substitution of the momentum transfer cross section for the elastic cross section is probably not too serious an approximation. This view is supported by Itikawa. The CO₂ data is more accurate, but the uncertainty in the scaling formula probably renders the distinction between momentum transfer cross section and elastic cross section irrelevant. Finally, the e - C₃H₈ scattering data of McCorkle et al.¹⁷ was used. In this case also, the momentum transfer cross sections were measured.

The energy differences ΔE of Na were taken to be the d-f splittings measured by Gallagher et al.¹⁸ The parameter γ in the Rb and Xe collisions were determined from Eq. (15), assuming

$$\Delta\delta \approx \delta_f \quad (18)$$

where $\delta_f = 0.02$ for Rb and 0.055 for Xe.

3. Cross Sections

Results for collisions of Na and Rb Rydberg atoms with rare gases are presented in Figures 4-9. The agreement for the case that the collision partner is He is especially good. Note that the present results for Na(nd) + He are determined using the scaling formula; they differ only slightly from the coupled channel and Born approximation results presented previously. The good agreement for He suggests that the Fermi pseudopotential is a rather good approximation when the low energy electron scattering has a weak dependence on energy. Also, the small polarizability of He supports the use of a short range (delta function) approximation to the e-He potential. For the collisions involving Ar and Ne the energy dependence of the electron scattering cross section does influence the predicted result for $n \sim 10-20$. The calculated cross sections are in reasonable agreement with the data in this range, suggesting that the approximate method of including the energy dependence [Eq. (13)] is at least qualitatively correct.

We have also applied the scaling formula to collisions involving more complicated partners. In these calculations the internal structure of the target is neglected, although it may of course influence the electron scattering cross sections used. The qualitative agreement observed between the calculations and experiment tends to suggest

that the elastic scattering of the electron by the target is the dominant mechanism of ℓ -mixing in these collisions as well as in those involving rare gases. Note that the formula is not intended to be used for a collision partner that has a charge or large dipole moment.

Figures 10 thru 13 show the calculated results for a number of molecular targets. The agreement with experiment is generally reasonable. The excellent results for $\text{Na(nd)} + \text{N}_2$ tend to confirm, as in the case of He, the reliability of the Fermi pseudopotential when the low energy electron scattering does not have a strong energy dependence.

It is interesting to consider the structure observed in the experimental data near $n = 15$ for $\text{Na(nd)} + \text{C}_3\text{H}_8$. We have considered what form of the elastic cross section σ_{el} would be necessary to lead to the observed form of $\sigma_{\ell\text{-mix}}(n)$, assuming the validity of Eq. (11). We found that the unusual structure in $\sigma_{\ell\text{-mix}}(n)$ for $n \sim 13-16$ could be fit by assuming an electron-propane elastic scattering cross section that exhibits a strong change of slope, but not a dip, at an electron energy 0.060 eV, which is the average electron kinetic energy for $n = 15$. This effective elastic cross section is about a factor of two less than σ_m of McCorkle et al.¹⁷ for $E > 0.060$ eV, but rises more sharply for $E < 0.060$ eV. In this region ($n \sim 15-17$) the size of the coupling strength parameter β is sensitive to two competing

factors. As n increases, A increases because of the rapid increase in σ_{e1} as the electron energy goes to zero. However, this is nearly counteracted by the factor $n^{-3.37}$ that reflects the weaker effect of the increasingly more diffuse electron cloud. The net effect is that the coupling strength teeters between these competing influences. The results of this analysis are only qualitative, of course, but they indicate that the unusual structure in the Rydberg cross section can be related to a plausible behavior of the corresponding electron scattering cross section.

IV CONCLUDING REMARKS

An approximate scaling formula for collisional angular momentum mixing of low- l Rydberg atoms has been determined that gives reasonable results for a wide variety of systems. Although the formula was determined using calculations that assumed the collision partner was a rare gas, qualitative agreement is also obtained for targets with internal structure. All the cross sections exhibit a maximum as a function of n , but the shape and position of the peak may vary considerably. For example, $\text{Rb} + \text{He}$ has a sharp peak at $n = 11$, while $\text{Xe} + \text{CO}_2$ has a very broad maximum for $n \sim 28$. The formulas obtained here show how such contrasting behavior may be qualitatively related to the energy level splittings of the Rydberg atom, the energy dependence of the electron scattering from the collision partner, and the relative velocity of the collision.

ACKNOWLEDGEMENTS

This work was supported by the Air Force Office of Scientific Research.

REFERENCES

1. T. F. Gallagher, S. A. Edelstein, and R. M. Hill, Phys. Rev. Lett. 35, 644 (1975).
2. T. F. Gallagher, S. A. Edelstein, and R. M. Hill, Phys. Rev. A 15, 1945 (1977).
3. T. F. Gallagher, S. A. Edelstein, R. E. Olson, W. E. Cooke, S. A. Edelstein, and R. M. Hill, Phys. Rev. A 16, 441 (1977).
4. R. E. Olson, Phys. Rev. A 15, 631 (1977).
5. A. Omont, J. Physique 38, 1343 (1977).
6. A. P. Hickman, Phys. Rev. A 18, 1339 (1978).
7. J. Derouard and M. Lombardi, J. Phys. B: Atom. Molec. Phys. 11, 3875 (1978).
8. A. P. Hickman, Phys. Rev. A 19, 994 (1979).
9. E. de Prunelé and J. Pascale, J. Phys. B: Atom. Molec. Phys. 12, 2511 (1979).
10. M. Hugon, F. Gounand, P. R. Fournier, and J. Berlande, J. Phys. B: Atom. Molec. Phys. 12, 2707 (1979).
11. M. Matsuzawa, J. Phys. B: Atom. Molec. Phys. 12, 3743 (1979).
12. K. A. Safinya and T. F. Gallagher, Phys. Rev. A, in press.
13. A. M. Arthurs and A. Dalgarno, Proc. R. Soc. (Lond) 256, 540 (1960).
14. R. E. Olson, Phys. Rev. A 6, 1822 (1972).
15. T. F. O'Malley, Phys. Rev. 130, 1020 (1963).
16. Y. Itikawa, Atomic Data and Nuclear Data Tables 14, 1 (1974).
17. D. L. McCorkle, L. G. Christophorou, D. V. Maxey, and J. G. Carter, J. Phys. B: Atom Molec. Phys. 11, 3067 (1978).

18. T. F. Gallagher, R. M. Hill and S. A. Edelstein, Phys. Rev. A 13, 1448 (1976).

TABLE 1

Values of $\sigma_{l\text{-mix}}$ as a function of n , v , and L obtained by coupled-channel calculations.

n	$v(\text{a.u.})$	$L(\text{a.u.})$	v	β	$\frac{\sigma_{l\text{-mix}}}{mn^4 a_0^2}$
4	6.867×10^{-4}	1.19	4.75	16.21	0.192
5	6.867×10^{-4}	1.19	3.82	7.64	0.387
6	6.867×10^{-4}	1.19	3.20	4.14	0.440
7	6.867×10^{-4}	1.19	2.75	2.46	0.402
8	6.867×10^{-4}	1.19	2.41	1.56	0.352
6	6.867×10^{-4}	0.595	3.20	2.07	0.324
6	6.867×10^{-4}	0.3	3.20	1.05	0.200
6	6.867×10^{-4}	0.15	3.20	0.523	0.082
6	6.867×10^{-4}	0.075	3.20	0.260	0.025
6	1.373×10^{-3}	1.19	1.60	2.07	0.535
6	4.856×10^{-4}	0.841	4.53	4.14	0.217
6	3.140×10^{-4}	0.544	7.00	4.14	0.102
6	3.140×10^{-4}	0.272	7.00	2.07	0.085
6	3.140×10^{-4}	0.137	7.00	1.04	0.055
6	3.140×10^{-4}	0.0686	7.00	0.523	0.024
6	3.140×10^{-4}	0.0343	7.00	0.260	0.0078
6	4.856×10^{-3}	0.421	4.53	2.07	0.171
6	1.717×10^{-3}	1.488	1.28	2.07	0.567
6	1.030×10^{-3}	0.892	2.14	2.07	0.462

TABLE 2

Values of the collision strength g as a function of β . For $\beta \leq 0.5$, $g = 0.715 \beta^2$. For $\beta \geq 3.0$, we arbitrarily set $g = 0.60$.

β	g
0	0
0.5	0.18
1.0	0.33
1.5	0.43
2.0	0.51
2.5	0.56
3.0	0.60

TABLE 3

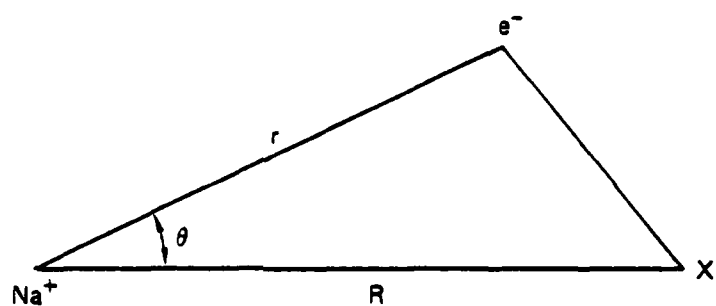
Values of the collision efficiency.

$\frac{n^2}{n_0} \frac{\Delta E}{\Delta v}$	f
0	1.00
1	0.99
2	0.91
3	0.78
4	0.65
5	0.54
6	0.45
7	0.38
8	0.32
9	0.28
10	0.25
11	0.22
12	0.19
13	0.18
14	0.17

FIGURE CAPTIONS

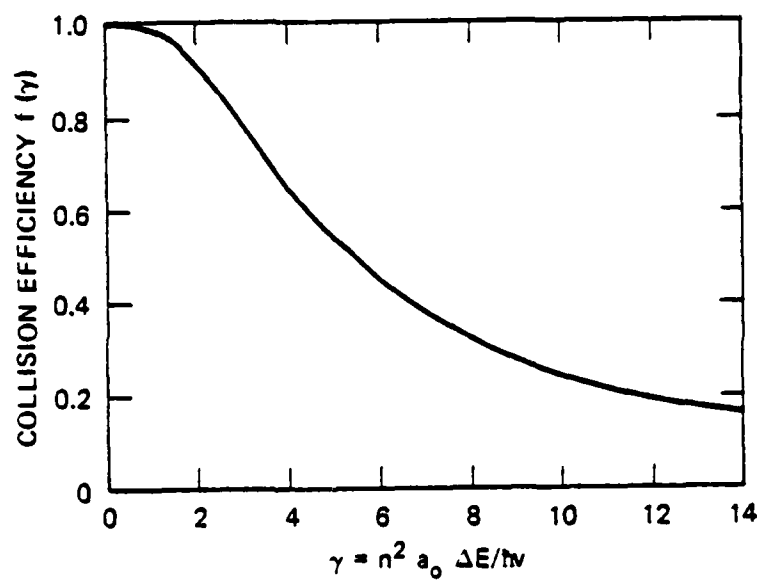
1. Schematic diagram of coordinates used to describe the Rydberg atom and its collision partner.
2. The function $f(\nu)$, which we interpret as the probability that a collision between the electron and the collision partner will cause a change of angular momentum level of the electron.
3. The function $g(\beta)$, which we interpret as the probability of encounter between the Rydberg electron and a collision partner.
4. The ℓ -mixing cross sections for $\text{Na}(\text{nd}) + \text{He}$. The calculation of de Prunelé and Pascale obtained upper and lower limits to the cross sections.
5. The ℓ -mixing cross sections for $\text{Na}(\text{nd}) + \text{Ne}$. The calculation of de Prunelé and Pascale obtained upper and lower limits to the cross sections.
6. The ℓ -mixing cross sections for $\text{Na}(\text{nd}) + \text{Ar}$. The calculation of de Prunelé and Pascale obtained upper and lower limits to the cross section.
7. The ℓ -mixing cross sections for $\text{Rb}(\text{nf}) + \text{He}$. The calculation of de Prunelé and Pascale obtained upper and lower limits to the cross sections.
8. The ℓ -mixing cross sections for $\text{Rb}(\text{nf}) + \text{Ar}$. The calculation of de Prunelé and Pascale obtained upper and lower limits to the cross sections.
9. The ℓ -mixing cross sections for $\text{Rb}(\text{nf}) + \text{Xe}$. The calculation of de Prunelé and Pascale obtained upper and lower limits to the cross sections.
10. The ℓ -mixing cross sections for $\text{Na}(\text{nd}) + \text{N}_2$. The calculation of de Prunelé and Pascale obtained upper and lower limits to the cross sections.
11. The ℓ -mixing cross sections for $\text{Na}(\text{nd}) + \text{CH}_4$.

12. The L -mixing cross sections for $\text{Na(nd)} + \text{C}_3\text{H}_8$. The unusual dip at $n=15$ is discussed in the text.
13. The L -mixing cross sections for $\text{Xe(nf)} + \text{CO}_2$.



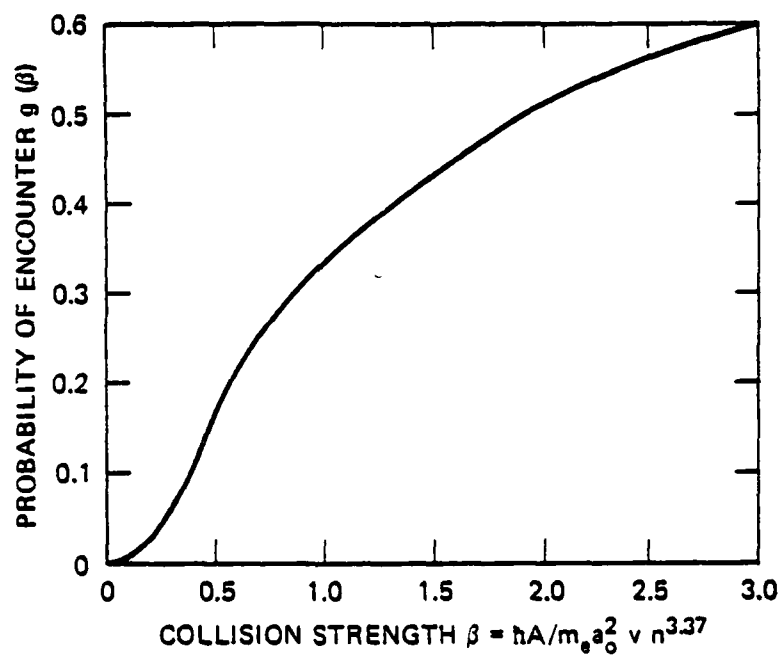
TA-330583-66R

Figure 1



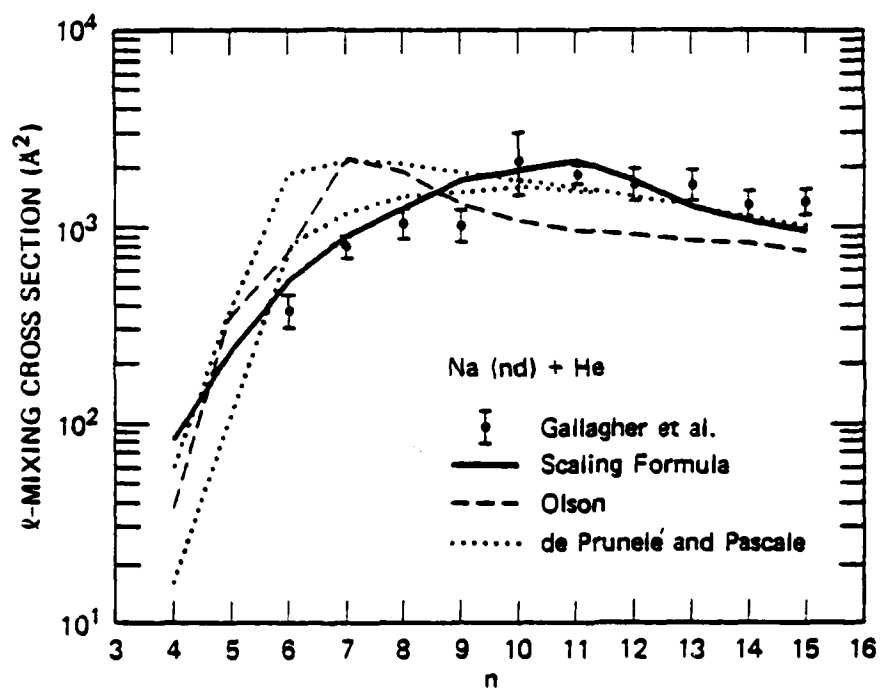
SA-4217-49R

Figure 2



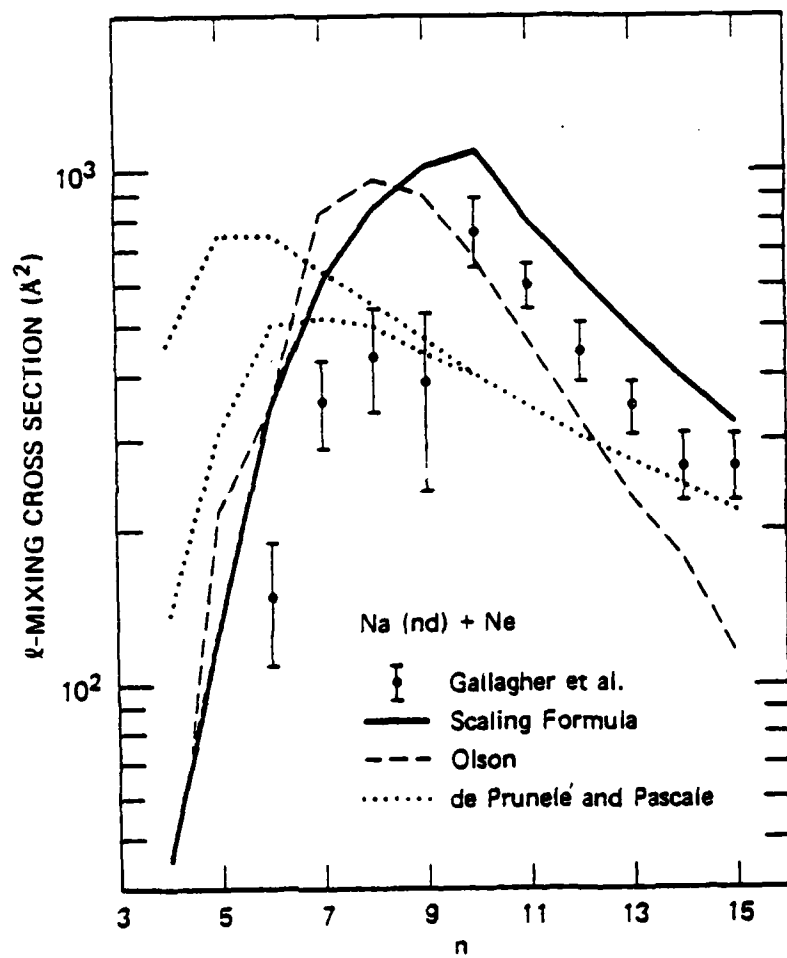
SA-4217-46R

Figure 3



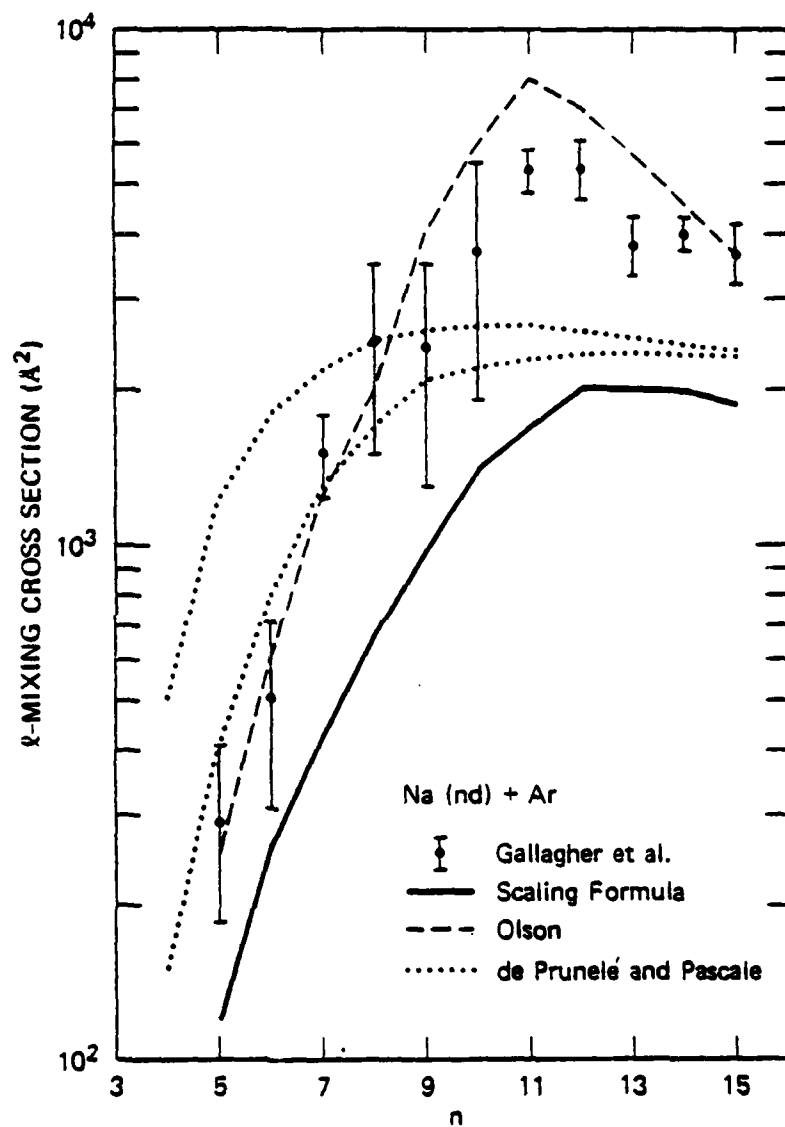
TA-330832-46R1

Figure 4



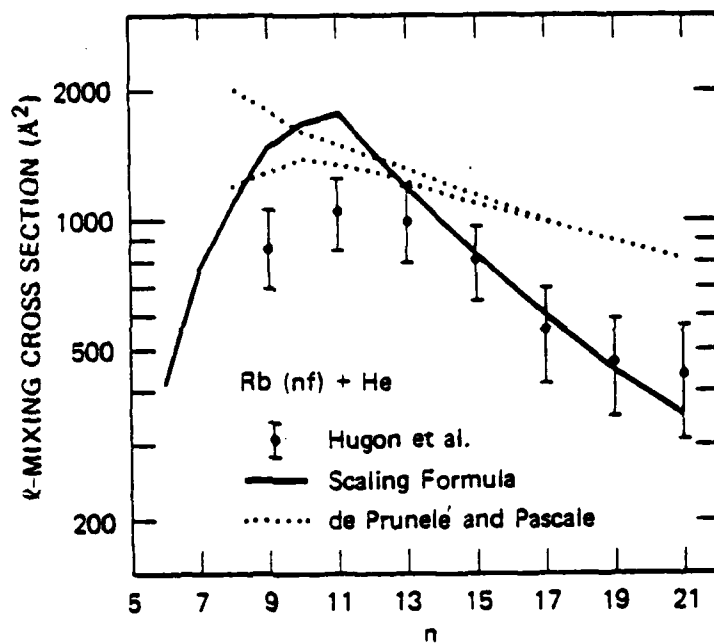
JA-1680-6

Figure 5



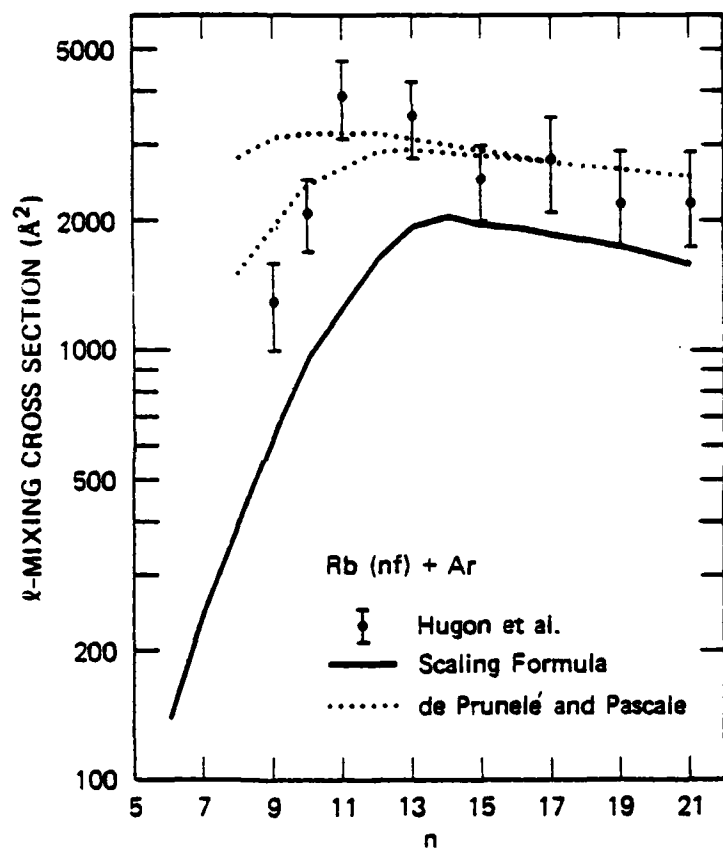
JA-1680-5

Figure 6



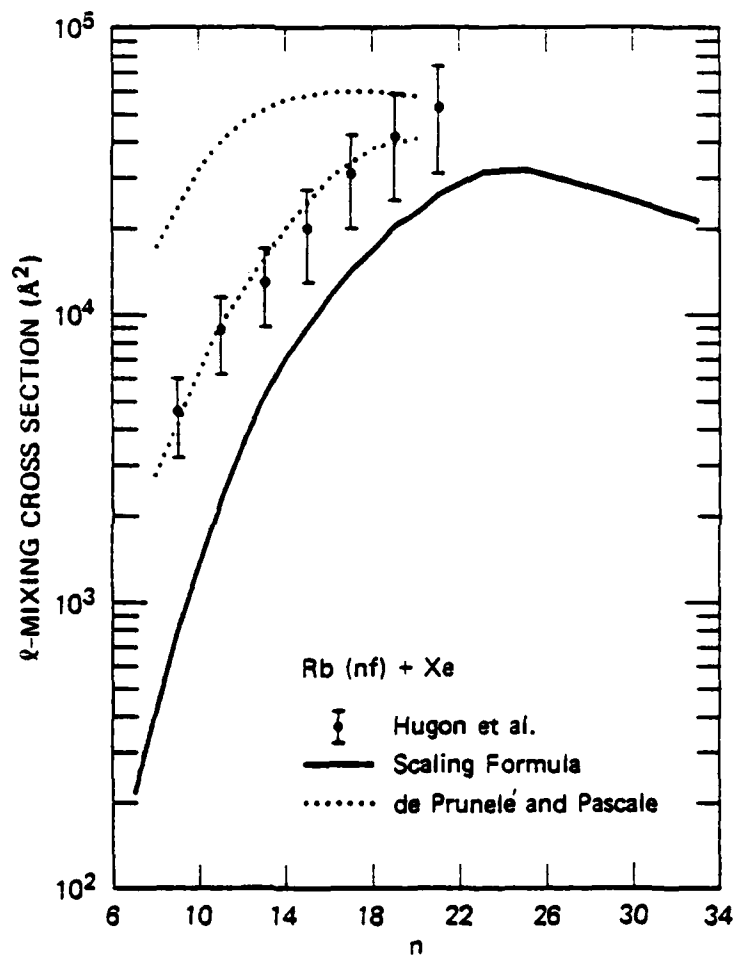
JA-1680-4

Figure 7



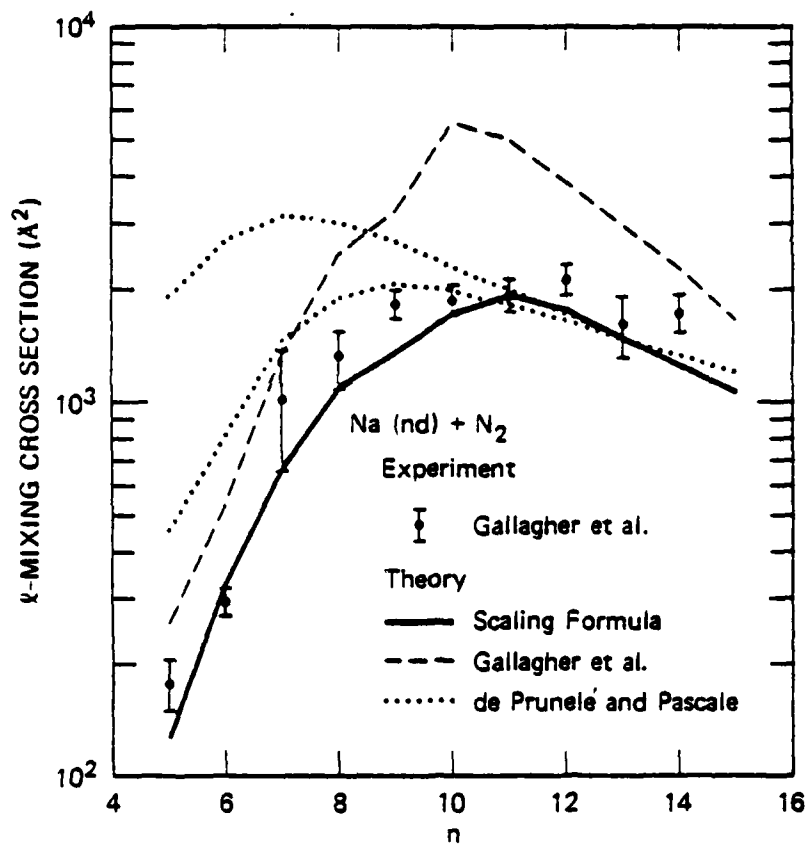
JA-1690-3

Figure 8



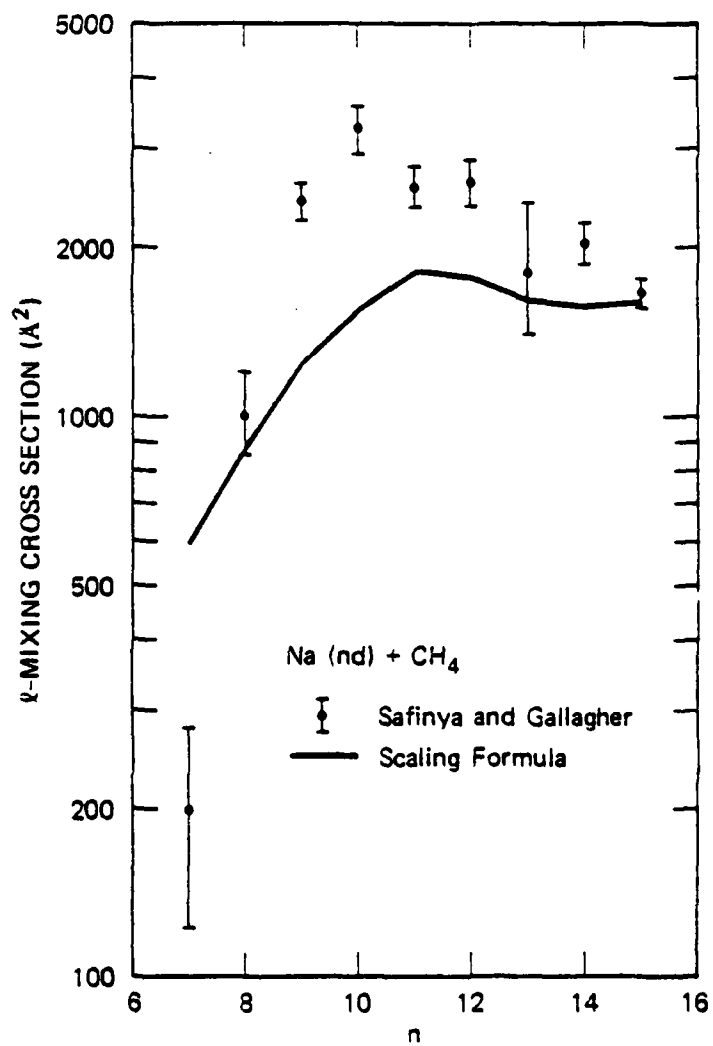
JA-1680-2

Figure 9



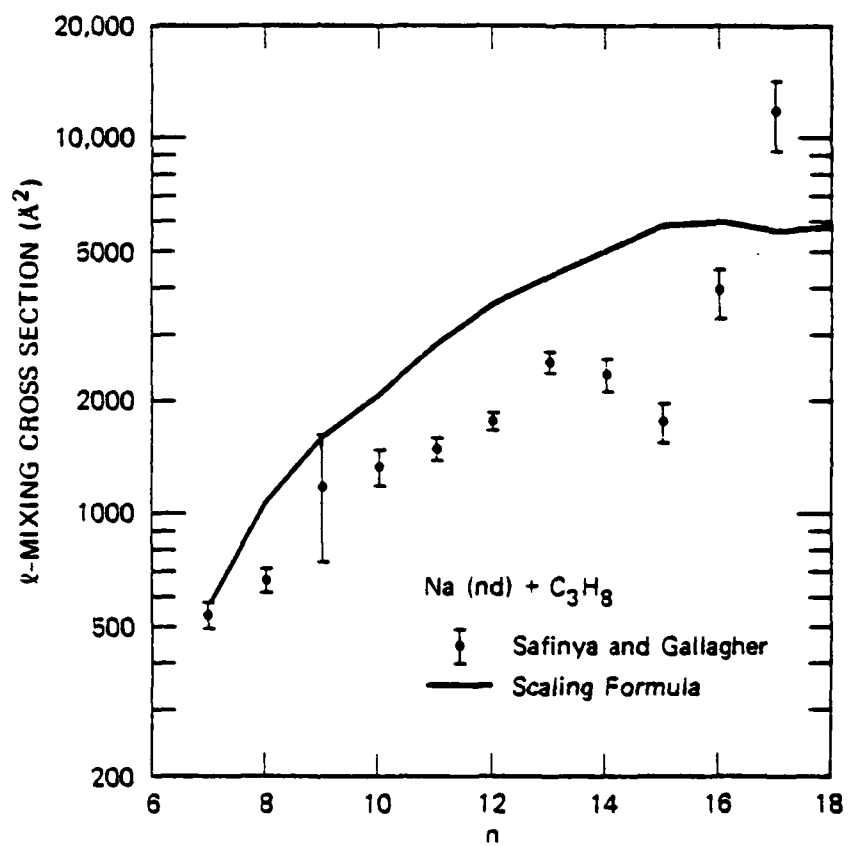
SA-4217-51R

Figure 10



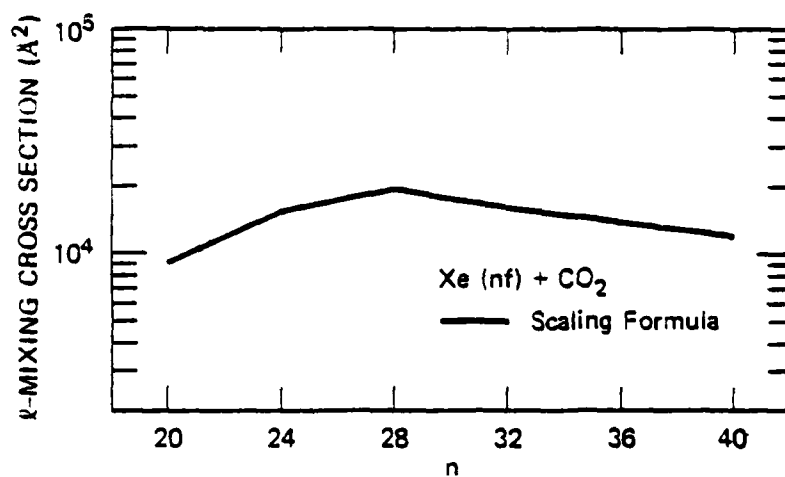
SA-4217-47R

Figure 11



SA-4217-52R

Figure 12



JA-1680-1

Figure 13

APPENDIX B

Excited States of CH^+ : Potential Curves
and Transition Moments

R. P. Saxon
Molecular Physics Laboratory
SRI International
Menlo Park, California 94025

K. Kirby
Harvard-Smithsonian Center for Astrophysics
60 Garden Street
Cambridge, Massachusetts 02138

B. Liu
IBM Research Laboratory
5600 Cottle Road
San Jose, California 95193

MP 80-43

Abstract

Wavefunctions and potential curves for the ground $X^1\Sigma^+$ state and eight excited states of $^1\Sigma^+$ and $^1\Pi$ symmetry of CH^+ have been obtained using ab initio configuration interaction (CI) methods. In order to take proper account of valence-Rydberg mixing, Rydberg functions were included in the basis set. The orbitals used in the set of reference configurations for the CI wavefunctions included both valence and Rydberg orbitals, determined from a multiconfiguration self-consistent field and a natural orbital calculation, respectively. Transition moments between the ground electronic state and the $2^1\Sigma^+$, $3^1\Sigma^+$, $A^1\Pi$ and $2^1\Pi$ states have been computed, and the importance of these states in photodissociation of CH^+ is discussed.

I. Introduction

The CH^+ molecule has been of great interest to astrophysicists ever since its discovery in diffuse interstellar clouds.¹ In particular, the abundance of CH^+ appears to be as much as 30 times larger than predictions based on probable formation and destruction mechanisms in interstellar clouds.² Also, many absorption lines observed in diffuse interstellar clouds remain unidentified.³ Transitions to excited states of CH^+ , not yet discovered in the laboratory, have been suggested as possible origins of some of these lines.⁴ A detailed understanding of the structure and radiative transitions of this molecule could lead to insights regarding these astrophysical observations.

The ground electronic state of CH^+ has $^1\Sigma^+$ symmetry and the oscillator strength of the only known dipole transition $A^1\Pi - X^1\Sigma^+$ has been calculated⁵ and measured.⁶ Accurate potential curves for the four lowest-lying electronic states, $X^1\Sigma^+$, $A^1\Pi$, $^3\Pi$ and $^3\Sigma^+$, dissociating to the lowest separated-atom limit $\text{C}^+(^2\text{P}) + \text{H}(^2\text{S})$ have been calculated by Green et al.⁷ No higher-lying excited states are reliably known, although Lorquet et al.⁸ produced some excited state potential curves showing a bound $^1\Sigma^+$ state dissociating to $\text{C}(^1\text{D}) + \text{H}^+$. Watson, Stewart and Dalgarno,⁹ using the random phase approximation, obtained large oscillator strengths for transitions in CH^+ from the $X^1\Sigma^+$ state to higher excited states. However, the calculation was carried out at only one internuclear separation, so

that the repulsive or attractive nature of these excited states was not determined.

In this work, we have undertaken a study to characterize those excited states of CH^+ , which, in dipole transitions from the ground state, can give rise to band spectra or to direct dissociation of the molecule. We have calculated potential curves, wavefunctions and transition moments for all eight states of $^1\Sigma^+$ or $^1\Pi$ symmetry lying within ~ 17 eV of the ground state. In Section II we discuss the basis set choice and the construction of configuration interaction wavefunctions which allow for adequate description of valence and Rydberg state interaction. Additional, larger calculations designed to test the results obtained are also described. The results of all the calculations as well as the astrophysical implications are detailed in Section III.

II. Calculations

The CH^+ excited states of interest in studies of the interstellar medium must lie within 13.6 eV of the ground state because there are no photons in the interstellar medium with $h\nu > 13.6$ eV due to the ionization of atomic hydrogen. However, in order to compute such states accurately the interaction with states lying somewhat higher in energy has to be considered. Figure 1 shows the lowest six CH^+ separated atom limits which give rise to states of singlet Σ or Π symmetry and the measured energy differences. The lowest two Rydberg limits $\text{C}(^1\text{P}, 2\text{p}3\text{s}) + \text{H}^+$ and $\text{C}^+(^2\text{P}) + \text{H}(2\text{s}, 2\text{p})$, lie within 0.2 eV of each other and within about

10 eV of the ground state asymptote. States arising from these Rydberg asymptotes may be of astrophysical interest. In addition, states arising from the lower-lying asymptotes probably experience some valence-Rydberg mixing at small internuclear separations. Thus, it is necessary to design a calculation which gives a balanced treatment of both valence and Rydberg states.

Electronic energies and wavefunctions were calculated using the configuration interaction (CI) method. Each wavefunction was expanded in an orthonormal, n -particle basis set of $C_{\infty v}$ symmetry-and equivalence-restricted configuration state functions (CSF). These CSF's were linear combinations of Slater determinants which have the appropriate molecular symmetry and multiplicity. The Slater determinants were constructed from an orthonormal set of molecular orbitals which were expanded in terms of an elementary basis set of Slater-type functions (STF) centered at the atomic nuclei.

The extended SCF basis set used in these calculations is given in Table 1. The (5s/4p) basis of Clementi and Roetti¹⁰ for $C(^3P)$ was augmented by two 3d functions, with exponents chosen to account for the distortion due to both long range electrostatic interaction and short range chemical interactions. Rydberg 3s and 3p functions with exponents optimized for the SCF energies of carbon atom Rydberg states 1P and 3D , respectively, were added to the set. The hydrogen atom basis was chosen to describe both the separated-atom and molecular-bonding regions, as

well as the Rydberg 2s and 2p limits. The molecular basis set consisted of 24 σ , 12 π and 3 δ functions.

In the construction of the CI wavefunctions, care was taken to treat Rydberg and valence states in an equivalent manner in order to properly describe valence-Rydberg mixing. The configuration lists for the $^1\Sigma$ and $^1\Pi$ symmetries consisted of all single and double excitations with respect to the lists of reference configurations given in Table 2, in which both valence and Rydberg orbitals were occupied. In order to dissociate the molecule correctly, in these configurations, the 3 σ and 4 σ orbitals, which asymptotically have the form $3\sigma = 2p_C + 1s_H$ and $4\sigma = 2p_C - 1s_H$, were treated equivalently. The 5 σ , 6 σ , 2 π and 3 π orbitals are Rydberg orbitals. The number of configurations in the CI wavefunction was 6808 for the Σ symmetry and 9573 for the Π symmetry.

For each internuclear separation, the orbitals for these calculations were determined by a four-step procedure designed to provide physically realistic Rydberg as well as valence orbitals. In the first step, valence σ orbitals were determined by a multiconfiguration self-consistent field (MCSCF) calculation on the $X^1\Sigma^+$ state which included the configurations $1\sigma^2 2\sigma^2 3\sigma^2$ and $1\sigma^2 2\sigma^2 4\sigma^2$, required for proper dissociation, along with the correlating configurations $1\sigma^2 3\sigma^2 1\pi^2$ and $1\sigma^2 4\sigma^2 1\pi^2$. With the σ orbitals frozen in the second step the valence π orbital was determined from a properly dissociating MCSCF calculation on the $A^1\Pi$ state which included the configurations $1\sigma^2 2\sigma^2 3\sigma 1\pi$ and $1\sigma^2 2\sigma^2 4\sigma 1\pi$. In the third step, two Rydberg

σ orbitals were obtained as natural orbitals from a frozen core two electron CI calculation for $^1\Sigma$ Rydberg states which included all configurations with one electron in the 3σ or 4σ orbital and one electron in an external σ orbital, i.e. $n\sigma$ for $n \geq 5$. In this calculation, six electronic states were obtained and the occupied Rydberg orbital from the lowest two states in which the Rydberg orbital was occupied was selected; i.e., one orbital was taken from each state. Finally, two Rydberg π orbitals were obtained in an analogous manner from a CI calculation for $^1\Pi$ Rydberg states which included all configurations with one electron in the 3σ or 4σ orbital and one electron in an external π orbital, i.e., $n\pi$ for $n \geq 2$.

The orbitals thus obtained were used for the CI calculations on both the Σ and Π symmetries. The calculations were performed at 25 internuclear separations between $R = 1.5 a_0$ and $20 a_0$.

A limited number of larger configuration interaction calculations were carried out to test whether certain improvements which could be made in these calculations would significantly affect the results. As will be discussed in the next section, the basis set used resulted in errors in asymptotic excitation energies as large as 0.4 eV. Therefore, in these extended calculations an enlarged basis set listed in Table 1 was employed. This set consisted of the (6s/4p) basis of Clementi and Roetti¹⁰ for $C(^3P)$, augmented by two 3d functions, two 3s and two 3p Rydberg functions and one 4f function. The diffuse 3d function was chosen to maximize the polarizability of the $C(^3P)$ atom and the tight 3d function to maximize

the energy lowering in a CI calculation on the CH^+ molecule ($^3\Sigma^-$ state). The tighter 3s and 3p Rydberg functions were optimized with respect to SCF energy of $\text{C}(^1\text{S})$ and $\text{C}(^3\text{D})$ respectively. Finally, the total energy of the $\text{CH}^+ ^3\Sigma^-$ state was found to be insensitive to the 4f exponent. No changes were made in the H basis functions in the enlarged basis set.

All of the reference configurations listed in Table 2 have the 2σ orbital doubly occupied although one of the asymptotes $\text{C}^+(1s^2 2s 2p^2 ^1\text{D}) + \text{H}^+$ under consideration has the carbon 2s orbital singly occupied. In the extended calculations, the 2σ orbital was included in the valence space and the configuration list was not limited by reference to a set of specific configurations. For the calculations on the $^1\Sigma^+$ symmetry, the valence set consisted of the 2σ , 3σ , 4σ and 1π orbitals, the Rydberg set included the 5σ , 6σ , 7σ and 2π orbitals and the remainder of the orbitals comprised the external set. The configuration list included all configurations generated by distributing (i) 4 electrons in the valence set and (ii) 3 electrons in the valence set and one in the Rydberg set, plus all single and double excitations with respect to the configurations in (i) and (ii). For calculations on the $^1\Pi$ symmetry, the Rydberg set consisted of only the 2π orbital. The 1σ core orbital was kept fully occupied in all configurations. This procedure resulted in 15454 configurations for the $^1\Sigma^+$ symmetry and 13063 configurations for the $^1\Pi$ symmetry.

The molecular orbitals used in the extended calculations were determined by the same four step procedure previously described.

Calculations of the five lowest $1\Sigma^+$ states and four lowest 1Π states were carried out at a limited number of internuclear separations. Results of these test calculations are presented and compared with the results of the calculation described previously.

The MCSCF calculations were performed using a program developed by J. Hinze. All other calculations were performed using the ALCHEMY system of programs developed by P. S. Bagus, B. Liu, A. D. McLean and M. Yoshimine.

III. Results and Discussion

A. Potential curves and asymptotes

In Figure 2, potential curves for the five lowest $1\Sigma^+$ and four lowest 1Π states of CH^+ are presented. The energies of these states as a function of internuclear distance are listed in Table 3. Of these nine states, only the $X^1\Sigma^+$, $A^1\Pi$ and $2^1\Sigma^+$ states are bound with respect to their asymptotic limits. Dissociation energies, equilibrium separations and spectroscopic constants for the X and A states are compared in Table 4 with the previous CI calculations of Green et al.⁷ and with experiment. Satisfactory agreement with both sets of values is observed. Discrepancies for the $A^1\Pi$ state are somewhat larger than those for the $X^1\Sigma^+$ state.

Excitation energies of the four asymptotes considered in this work, relative to the lowest asymptote $\text{C}^+(^2\text{P}) + \text{H}(^2\text{S})$ at the separated atom limit of $R = 20a_0$ are given in Table 5. The excitation energies of the

$C(^1D) + H^+$ and the $C(^1S) + H^+$ asymptotes are each larger by 0.4 eV than the experimental values. However, the calculated splitting between the two states of neutral carbon $C(^1D)$ and $C(^1S)$ is exactly equal to the spectroscopic value. In effect, the error in the ionization potential of the carbon atom is ~ 0.4 eV in this calculation. Excitation energies are given critical attention in the comparison between these values and the results of the extended CI calculations presented in the next section.

B. Extended CI Results

The extended CI calculations were carried out at the $R = 20a_0$ asymptote and at three points in the interaction region. Excitation energies for these calculations are also listed in Table 5. Discrepancies in excitation energies for the first two excited limits are lowered from 0.4 eV to 0.2 - 0.25 eV. There is, however, no change in the excitation energy of the carbon Rydberg limit, $C(^1P) + H^+$. Asymptotically, the total energy from the extended calculations is lower by 3 millihartrees for the $X^1\Sigma^+$ state and by 2 mh for the $A^1\Pi$ state.

Interaction potential curves were compared at internuclear distances of 1.9, 2.2, and 3.4 a_0 . For all nine states, the maximum energy discrepancy observed was 0.3 eV; all others are ≤ 0.2 eV. In the extended calculations, near the potential minimum, the $A^1\Pi$ state was lowered by ~ 0.2 eV while the $X^1\Sigma^+$ state was virtually unchanged. That the $A^1\Pi$ is less well determined in the main calculations reported here than the $X^1\Sigma^+$ state is further confirmed by the greater discrepancy with respect

to experimental values of the spectroscopic constants in Table 4 for the $A^1\Pi$ state than for the $X^1\Sigma$ state. However, in general, energy shifts of this magnitude have little effect on the qualitative features of the potential curves. Thus it was concluded that the main calculations reported here realistically characterize the excited states of CH^+ .

C. Discussion of Potential Curves

In using potential curves shown in Figure 2 to interpret physical processes, the most reliable information is obtained by shifting the curves so that their asymptotes have the spectroscopic separation, given in Table 3.

The avoided crossing of the $2^1\Sigma^+$ and $3^1\Sigma^+$ states gives rise to a hump in the $2^1\Sigma^+$ state with a height of ~ 0.5 eV between 3 and 4 a_0 . A cursory search for quasi-bound levels on an energy grid of 5×10^{-5} hartrees, led to three resonances at 0.296, 0.466 and 0.588 eV above the separated atom limit. The $2^1\Sigma^+$ state appears to experience a small $1/R^4$ attraction at large R with an energy minimum of about 0.2 eV at $R \approx 6.2 a_0$. This, however, is well outside the Franck-Condon region of the ground state.

The two highest $^1\Sigma^+$ and $^1\Pi$ states calculated also appear to interact. The $4^1\Sigma^+$ and $5^1\Sigma^+$ states (as well as the $3^1\Pi$ and $4^1\Pi$ states) are very close in energy at $R \approx 3.5 a_0$, creating ripples in the potential curves. The $5^1\Sigma^+$ also appears to have a quasi-bound vibrational level about 2.8 eV above the separated atom limit.

It is clear that, with the exception of the quasi-bound vibrational levels mentioned above, no new band spectra of CH^+ are to be found. The excited states will be important, however, for photodissociation. With the asymptotes shifted to agree with experiment, the vertical excitation energies at $R = 2.1 a_0$ from the $v=0$ level of the ground state to the $2^1\Sigma^+$, $3^1\Sigma^+$ and $2^1\Pi$ states are 8.02, 12.92 and 13.58 eV, respectively. These states may be significant in photodissociating CH^+ in the interstellar medium. In comets where a large amount of CH^+ can be observed and where there is no Lyman cut-off of the solar photons, even higher states may be important in the photodestruction of CH^+ .

D. Transition Moments

The electric dipole moments for transitions between the ground state and the $2^1\Sigma^+$, $3^1\Sigma^+$, $1^1\Pi$ and $2^1\Pi$ states of CH^+ are given as a function of R in Table 6 and Figure 3. Properties, such as the transition moment, tend to be more sensitive than the energy to the quality of the wavefunction used to calculate them. When the transition moments from the main calculations were compared with the results of the extended CI calculations there was excellent agreement for transitions to the $2^1\Sigma^+$, $3^1\Sigma^+$, $1^1\Pi$ and $2^1\Pi$ states but fairly large discrepancies for transitions to the higher states, $4^1\Sigma^+$, $5^1\Sigma^+$, $3^1\Pi$ and $4^1\Pi$. Since one of the main improvements in the extended CI calculations is the inclusion, in effect, of 2s excited reference configurations and since the $\text{C}^+(^2D)$ asymptote to which the $4^1\Sigma^+$ and $3^1\Pi$ dissociate is a 2s excited configuration, this observation

is reasonable. We, therefore, present transition moments only for the lower states, which include all states assessible in the interstellar medium.

Our values for the X-A transition moment are generally within 20% of those of Yoshimine et al.⁵ which was used to predict an oscillator strength for transitions between the lowest vibrational levels of each state in excellent agreement with a subsequent experimental measurement.⁶ At $R = 20 a_0$ the transition moments between the ground state and the first two excited states of each symmetry are zero, consistent with the fact that there is no dipole transition possible between $C^+(^2P) + H(^2S)$ and either $C(^1D) + H^+$ or $C(^1S) + H^+$. At $R = 2.1 a_0$, transition moments to the $3^1\Sigma^+$ and $2^1\Pi$ are relatively large, in agreement with the finding of Watson et al.⁹ The sum of the electronic oscillator strengths to all the excited states presented here is 1.08. There are many peaks and dips in the transition moments for the higher states which are indicative of the changes of character in the wavefunction occurring due to valence-Rydberg mixing.

Photodissociation cross sections to the $2^1\Sigma^+$, $3^1\Sigma^+$ and $2^1\Pi$ and excited states will be reported separately.¹¹ The photodissociation cross section and rates for the A-X transition have been calculated by Uzer and Dalgarno,¹² using the transition moments of Yoshimine et al.⁵

E. Summary

Potential curves for a dipole transition moments to excited states of CH^+ have been computed using large CI wavefunctions for both $1\Sigma^+$ and 1Π symmetry. In order to obtain accurate valence-Rydberg interactions, a Slater basis set containing Rydberg functions was used and both valence and Rydberg molecular orbitals were included in the reference set of configurations from which single and double excitations were allowed. All the excited states except for the $A^1\Pi$ were found to be repulsive in the range of internuclear separations for which the $X^1\Sigma^+$ is bound ($1.5 a_0 - 5.5 a_0$). Thus, these calculations show that none of the unidentified absorption lines observed in diffuse interstellar clouds can be attributed to CH^+ . Several resonances (quasi-bound vibrational levels) due to humps in the $2^1\Sigma^+$ and $3^1\Sigma^+$ potential curves may be observable.

From inspection of the transition moments, it appears that photo-dissociation cross sections to the $2^1\Pi$ and $3^1\Sigma^+$ will be large. These states, in addition to the $2^1\Sigma^+$, may be significant in photodissociating CH^+ in the interstellar medium.

Acknowledgement

One of the authors (R.P.S.) was supported by the Air Force Office of Scientific Research under Contract FF44620-75-C-0073.

REFERENCES

1. See for instance A. E. Douglas and G. Herzberg, Ap. J. 94, 381 (1941) and A. E. Douglas and G. Herzberg, Can. J. Phys. 20, 71 (1942) and references to earlier work contained therein.
2. J. H. Black and A. Dalgarno, Ap. J. Suppl. 34, 405 (1977) and a review of the CH/CH⁺ situation by A. Dalgarno in Atomic Processes and Applications, p. 110, 1976, North-Holland: Amsterdam, Ed. by P. G. Burke and B. L. Moiseiwitsch.
3. D. C. Morton, Ap. J. 197, 85 (1975).
4. A. Dalgarno, private communication.
5. M. Yoshimine, S. Green, and P. Thaddeus, Ap. J. 183, 899 (1973).
6. P. Erman, Ap. J. Letts. 213, L89 (1977) and J. Brzozowski, N. Elander, P. Erman, and M. Lyrra, Ap. J. 193, 741 (1974).
7. S. Green, P. S. Bagus, B. Liu, A. D. McLean, and M. Yoshimine, Phys. Rev. A5, 1514 (1972).
8. A. J. Lorquet, J. C. Lorquet, H. Wankenne, J. Momigny, and H. Lefebvre-Brion, J. Chem. Phys. 55, 4053 (1971).
9. D. K. Watson, R. F. Stewart, and A. Dalgarno, J. Chem. Phys. 64, 4995 (1976).
10. E. Clementi and C. Roetti, At. Data Nucl. Data Tables 14, 177 (1974).
11. K. Kirby, W. Roberge, R. P. Saxon, and B. Liu, to be published Ap. J.
12. T. Uzer and A. Dalgarno, Chem. Phys. 32, 301 (1978).
13. Données Spectroscopiques Relatives aux Molécules Diatomiques, edited by B. Rosen (Pergamon, Oxford, 1971).

Table 1
Slater Basis Set for CH⁺
Extended Calculations

C			H	
nl	$\zeta(a_0^{-1})$	Extended Calculations $\zeta(a_0^{-1})$	nl	$\zeta(a_0^{-1})$
1s	9.25013	9.48256	1s	1.7
1s	5.53875	5.43599	1s	1.0
2s	5.30567	4.20096	1s	0.5
2s	2.04126	2.68435	2s	1.0
2s	1.30552	1.52427	2s	0.5
2s		1.05749		
3s	1.29478	0.5856	2p	2.0
3s	0.58380	0.3	2p	1.0
2p	6.53286	6.51003	2p	0.5
2p	2.60786	2.60051	3d	2.0
2p	1.44037	1.44361		
2p	0.96499	0.98073		
3p	1.23210	0.4855		
3p	0.47960	0.24		
3d	2.34	2.009		
3d	1.24	0.95		
4f		2.3		

Table 2

Reference Configurations for CI Calculations

$\frac{1}{\Sigma}^{+}$	$\frac{1}{\pi}$
$1\sigma^2 2\sigma^2 3\sigma^2$	$1\sigma^2 2\sigma^2 3\sigma 1\pi$
$1\sigma^2 2\sigma^2 4\sigma^2$	$1\sigma^2 2\sigma^2 4\sigma 1\pi$
$1\sigma^2 2\sigma^2 3\sigma 4\sigma$	$1\sigma^2 2\sigma^2 3\sigma 2\pi$
$1\sigma^2 2\sigma^2 1\pi^2$	$1\sigma^2 2\sigma^2 4\sigma 2\pi$
$1\sigma^2 2\sigma^2 3\sigma 5\sigma$	$1\sigma^2 2\sigma^2 3\sigma 3\pi$
$1\sigma^2 2\sigma^2 3\sigma 6\sigma$	$1\sigma^2 2\sigma^2 4\sigma 3\pi$
$1\sigma^2 2\sigma^2 4\sigma 5\sigma$	
$1\sigma^2 2\sigma^2 4\sigma 6\sigma$	

Table 3
POTENTIAL CURVES FOR $1\Sigma^+$ AND 1Π STATES OF CH^+
GIVEN IN HARTREES RELATIVE TO THE ASYMPTOTIC ENERGY OF EACH STATE^a

$R(a_0)$	$1\Sigma^+$	$2\Sigma^+$	$3\Sigma^+$	$4\Sigma^+$	$5\Sigma^+$
1.5	-0.03335	0.16712	0.32063	0.26491	0.29191
1.6	-0.07786	0.11777	0.26916	0.21644	0.23624
1.7	-0.10867	0.08192	0.23058	0.18132	0.19408
1.8	-0.12924	0.05614	0.20125	0.15576	0.16234
1.9	-0.14210	0.03790	0.17845	0.13661	0.13909
2.0	-0.14920	0.02530	0.16021	0.12128	0.12323
2.1	-0.15197	0.01690	0.14512	0.10849	0.11326
2.2	-0.15154	0.01163	0.13221	0.09807	0.10726
2.4	-0.14424	0.00737	0.11065	0.08353	0.10193
2.6	-0.13200	0.00798	0.09286	0.07490	0.10080
2.8	-0.11762	0.01079	0.07771	0.06945	0.10040
3.0	-0.10275	0.01418	0.06447	0.06523	0.09274
3.2	-0.08836	0.01722	0.05257	0.06080	0.07332
3.4	-0.07500	0.01935	0.04169	0.05478	0.05740
3.6	-0.06293	0.02027	0.03183	0.04600	0.04781
3.8	-0.05225	0.01979	0.02331	0.03623	0.04273
4.0	-0.04297	0.01788	0.01644	0.02753	0.03996
4.3	-0.03151	0.01290	0.00934	0.01738	0.03820
4.6	-0.02270	0.00692	0.00520	0.01039	0.03748
5.0	-0.01433	-0.00003	0.00217	0.00468	0.03519
5.5	-0.00793	-0.00541	0.00020	0.00117	0.02858
6.0	-0.00441	-0.00759	-0.00083	-0.00024	0.01954
7.0	-0.00154	-0.00711	-0.00148	-0.00075	0.00168
8.0	-0.00068	-0.00501	-0.00129	-0.00063	-0.01080

20.0 -0.00000 0.14672 0.19880 0.35102 0.36497

$R(a_0)$	1Π	2Π	3Π	4Π
1.5	0.10645	0.44383	0.26283	0.29568
1.6	0.06008	0.38467	0.20883	0.24415
1.7	0.02710	0.33672	0.17097	0.20622
1.8	0.00402	0.29822	0.14410	0.17786
1.9	-0.01175	0.26714	0.12496	0.15373
2.0	-0.02215	0.24156	0.11132	0.12767
2.1	-0.02865	0.21984	0.10152	0.10336
2.2	-0.03234	0.20060	0.09394	0.08342
2.4	-0.03438	0.16603	0.07421	0.06593
2.6	-0.03266	0.13472	0.05958	0.06166
2.8	-0.02965	0.10713	0.05349	0.05991
3.0	-0.02655	0.08373	0.05126	0.05841
3.2	-0.02267	0.06644	0.05273	0.05635
3.4	-0.01992	0.05146	0.04998	0.05425
3.6	-0.01746	0.03954	0.04393	0.05256
3.8	-0.01525	0.03002	0.03592	0.05071
4.0	-0.01326	0.02237	0.02787	0.04824
4.3	-0.01068	0.01355	0.01780	0.04347
4.6	-0.00854	0.00719	0.01065	0.03809
5.0	-0.00626	0.00157	0.00477	0.03103
5.5	-0.00420	-0.00223	0.00115	0.02335
6.0	-0.00281	-0.00379	-0.00031	0.01710
7.0	-0.00132	-0.00384	-0.00083	0.00708
8.0	-0.00068	-0.00282	-0.00063	-0.00149

20.0 -0.00069 0.14817 0.35221 0.37578

^aThe asymptotic energy for each state is taken to be the calculated energy at $R = 20 a_0$. The energies for $R = 20 a_0$ are given relative to the calculated $1\Sigma^+$ asymptote of -37.87038857 hartrees. $1 a_0 = 0.52918 \text{ \AA}$; 1 hartree = 27.2116 eV.

Table 4

Spectroscopic Constants for $\text{CH}^+ \text{X}^1\Sigma^+$ and $\text{A}^1\Pi$ States

	This Work	Green et al. (Ref. 7)	Experiment (Ref. 13)
$\text{X}^1\Sigma^+$			
$R_e (a_0)$	2.133	2.136	2.137
$D_e (\text{eV})$	4.140	4.11	$4.27^a \pm 0.02$
$\Delta G_{1/2} (\text{cm}^{-1})$	2743		2740
$\text{A}^1\Pi$			
$R_e (a_0)$	2.381	2.332	2.333
$D_e (\text{eV})$	0.936	1.069	1.29^c
$\omega_e (\text{cm}^{-1})$	1526^b		1865^d
T_e	25690	24970	24033^e

a) $D_0^0 + \omega_e/2$ using values in Ref. 13

b) Using 4 vibrational levels

c) Using experimental T_0 , D_0^0 for X state and $\omega_e/2$ for A state

d) Applies to $v \leq 2$

e) Using experimental T_0 and $\omega_e/2$ for X and A states.

Table 5

Excitation Energies Relative to $C^+(^2P) + H(^2S)^a$ in eV

	1_{Σ}^+	Extended Calculations	1_{Π}	Extended Calculations	Spectroscopic
$C(^1P) + H^+$	9.93	9.93	10.22	10.22	10.023
$C^+(^2D) + H(^2S)$	9.55	9.44	9.58	9.44	9.290
$C(^1S) + H^+$	5.41	5.28			5.022
$C(^1D) + H^+$	3.99	3.82	4.03	3.83	3.602

a) Asymptote ($R=20a_0$) for $X^1_{\Sigma}^+$ state.

Table 6
CH⁺ Transition Dipole Moments

R	$\langle X^1\Sigma^+ z 2^1\Sigma^+ \rangle$	$\langle X^1\Sigma^+ z 3^1\Sigma^+ \rangle$	$\langle X^1\Sigma^+ \frac{x+iy}{\sqrt{2}} A^1\Pi \rangle$	$\langle X^1\Sigma^+ \frac{x+iy}{\sqrt{2}} 2^1\Pi \rangle$
1.5	0.2655	-0.3846	-0.4062	0.6202
1.6	0.2509	-0.4680	-0.3842	0.6731
1.7	0.2345	-0.5588	-0.3611	0.6873
1.8	0.2165	-0.6563	-0.3373	0.6873
1.9	0.1966	-0.7592	-0.3128	0.6781
2.0	0.1747	-0.8653	-0.2881	0.6592
2.1	0.1507	-0.9712	-0.2634	0.6287
2.2	0.1244	-1.0738	-0.2389	0.5862
2.4	0.0633	-1.2591	-0.1919	0.4762
2.6	-0.0110	-1.4105	-0.1492	0.3658
2.8	-0.1012	-1.5277	-0.1128	0.2782
3.0	-0.2102	-1.6118	-0.0833	0.2116
3.2	-0.3410	-1.6617	-0.0563	0.1561
3.4	-0.4958	-1.6736	-0.0380	0.1137
3.6	-0.6744	-1.6415	-0.0246	0.0790
3.8	-0.8694	-1.5598	-0.0151	0.0507
4.0	-1.0600	-1.4308	-0.0088	0.0276
4.3	-1.2777	-1.1888	-0.0032	0.0013
4.6	-1.3743	-0.9608	-0.0008	0.0165
5.0	-1.3510	-0.7363	-0.0003	0.0301
5.5	-1.1880	-0.5576	-0.0008	0.0359
6.0	-0.9721	-0.4409	-0.0015	0.0346
7.0	-0.5783	-0.2869	-0.0017	0.0248
8.0	-0.3173	-0.1820	-0.0013	0.0151
20.0	0.0002	0.0003	0.0000	0.0001

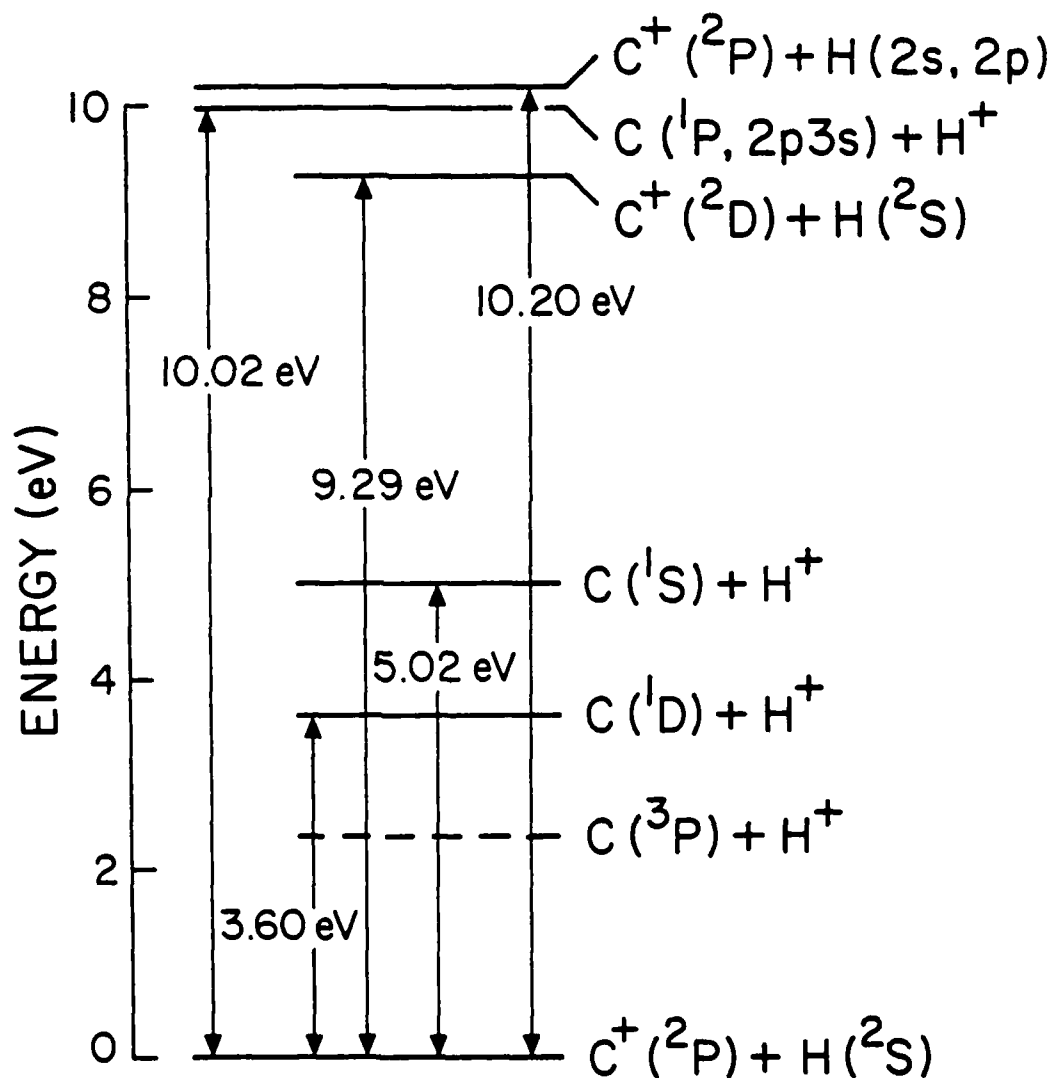
Figure Captions

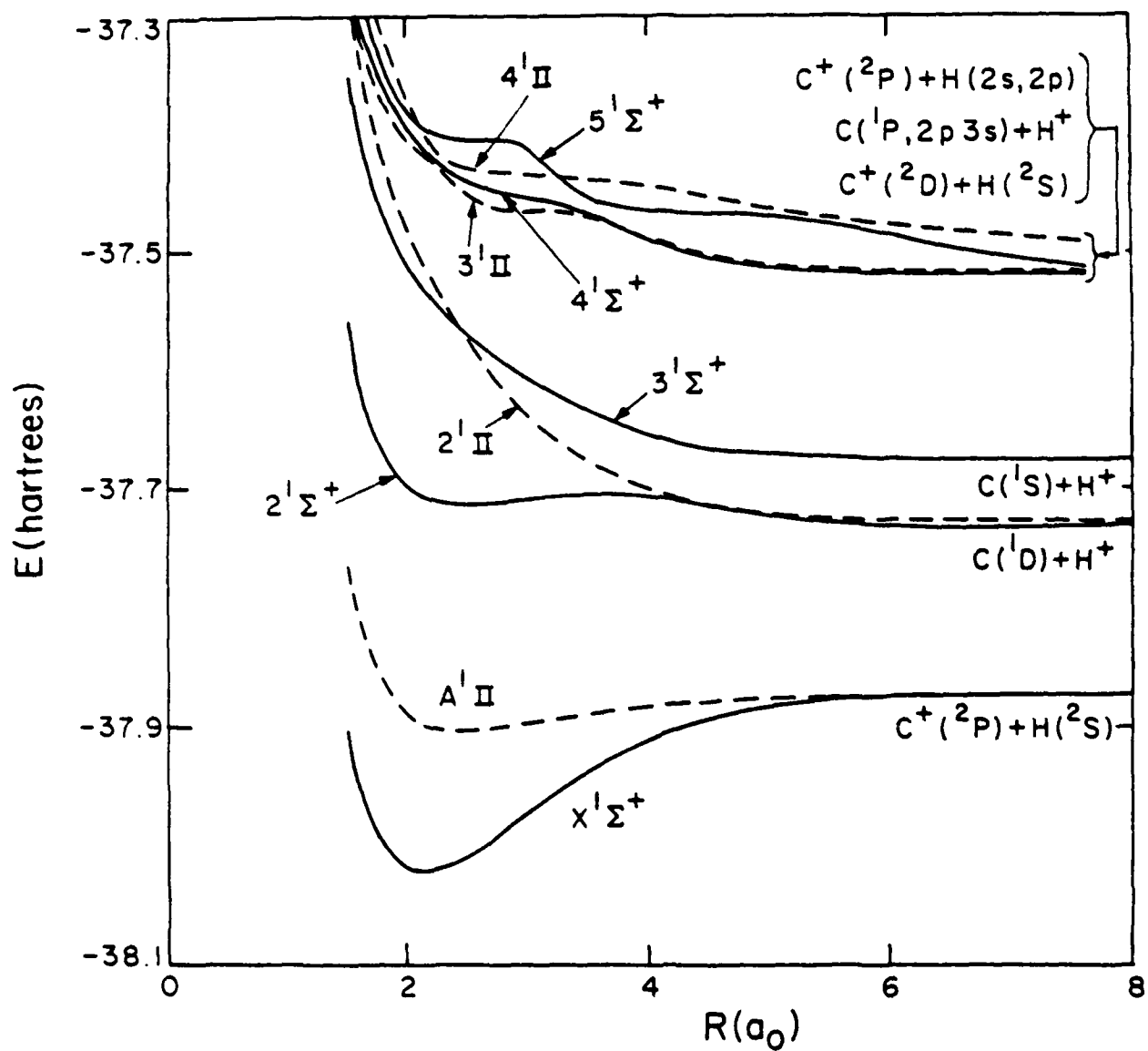
Figure 1: Separated-atom limits giving rise to $1\Sigma^+$ or 1Π states of CH^+ . Experimental energy separations are shown as taken from tables compiled by C. E. Moore, NBS circular 467, 1949.

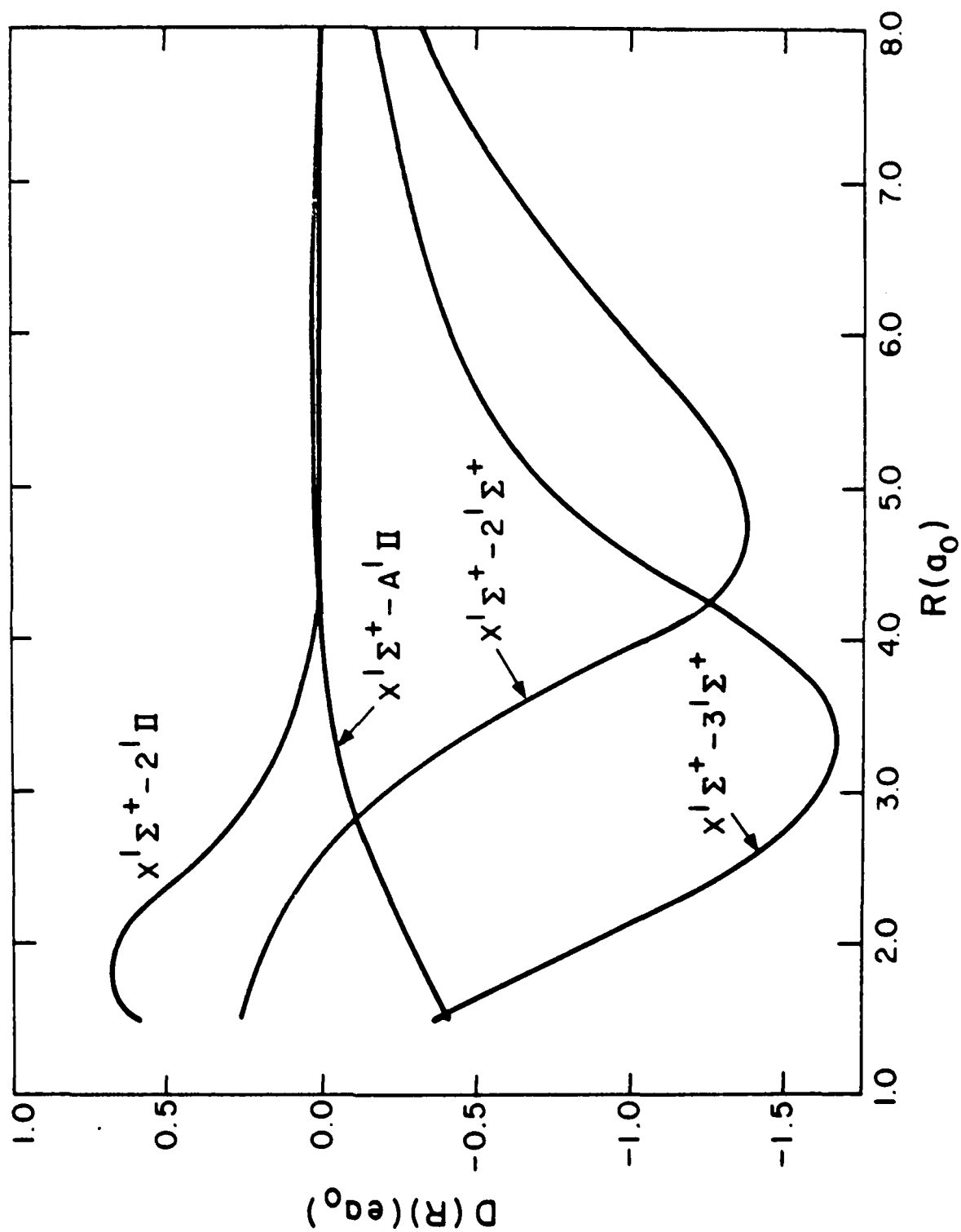
Figure 2: Potential curves of CH^+ : five of $1\Sigma^+$ symmetry and four of 1Π symmetry.

Figure 3: Transition moments from the ground state to the $21\Sigma^+$, $31\Sigma^+$, $A1\Pi$ and 21Π states of CH^+ as a function of internuclear separation. The relative signs of the transition moments are arbitrary.

CH⁺ ASYMPTOTES







APPENDIX C

COMPARISON OF ION PAIR FORMATION IN THE SYSTEMS $\text{Ar}^* + \text{I}_2$ and $\text{K} + \text{I}_2$

A. P. Hickman and Keith T. Gillen
Molecular Physics Laboratory
SRI International
Menlo Park, California 94025

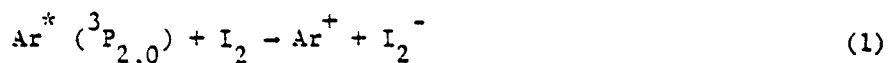
ABSTRACT

A simple model that has been used extensively by Los and coworkers to treat ion pair formation in collisions of alkali atoms with diatomic molecules is extended to include continuum coupling via a competing Penning ionization channel. This extended model is then used to calculate the differential cross sections for ion pair formation for the system $\text{Ar}^* + \text{I}_2$ over the energy range 28-154 eV and to compare with a previous treatment of $\text{K} + \text{I}_2$. In the absence of significant competition from continuum processes, Ar^* is expected to behave in a manner similar to K, since the active electron is an unpaired 4s electron in both cases. We perform model calculations for $\text{Ar}^* + \text{I}_2$ to investigate the effects of varying the potential curves and charge exchange matrix elements and of including a continuum coupling function $\Gamma(R)$. Comparison with previous calculations for $\text{K} + \text{I}_2$ suggests increased repulsion on the $\text{Ar}^* - \text{I}_2$ surfaces relative to those of $\text{K} - \text{I}_2$. The competing mechanisms of excitation transfer and Penning ionization may have a small effect upon the ion pair angular distributions.

MP 80-33

I INTRODUCTION

The study of a pair of generally similar reactions enables one to isolate subtle effects that arise specifically from the differences between the two systems. Recent measurements of the differential cross section for ion pair formation in collisions between halogen molecules and alkali atoms or metastable rare gas atoms provide such an opportunity. Over the energy range 30-150 eV, all of the major features observed¹ in the angular distribution for the reaction



can be correlated with those observed²⁻⁴ in the analogous reaction



However, there are differences in the ratios of the intensities of various features and in the position of the rainbow angle. The general similarity is consistent with the fact that both K and $\text{Ar}^* (^3\text{P})$ have an active, unpaired 4s electron. The observed differences between the two reactions should be related to the inner shell vacancy in Ar^* and to the additional competing channels energetically accessible to the system, including Penning ionization:



In this paper we present model calculations designed to elucidate the causes of the observed differences in the scattering data.

Ion-pair formation in the alkali-halogen system has been extensively investigated⁵⁻⁷ both experimentally and theoretically. These reactions have been modelled quite successfully by Los and coworkers^{5,6} using classical trajectory surface-hopping techniques^{8,9} that demonstrate the essential features of the reaction mechanism leading to ion-pair production. Here we have modified and extended those model calculations to include coupling to the continuum (reaction (3)). We estimate the autoionization rate $\Gamma(R)$ using a simplified form of a technique proposed recently by Miller and Morgner.¹⁰ We are therefore able to perform quantitative calculations that examine the effect of competing channels upon the ion pair distributions in reaction (1).

In Section II we present the details of the model calculations and discuss the inclusion of continuum coupling. Our results are presented and discussed in Section III, and Section IV contains a summary.

II THEORY

A. Summary of the Model

We have adopted the theoretical approach developed by Los and co-workers,^{2,5,6} which is a classical-trajectory, surface-hopping model^{8,9} with the following additional approximations:

1. Simple analytic potentials are constructed from pairwise interactions for the covalent electronic state $K + I_2$ and for the ionic state $K^+ + I_2^-$.
2. The cross sections are obtained as the average of cross sections for various orientations of the target molecule. The axis of this target is assumed not to rotate during the collision. Molecular vibration, however, is included, as explained below.
3. For each trajectory, the classical vibration of the molecule is calculated numerically assuming Morse potentials, and the deflection of the projectile is obtained analytically using classical perturbation theory.

An essential feature of the model is that the ionic and covalent surfaces cross at an Ar^*-I_2 distance R that depends on the vibrational coordinate of the molecule. This fact influences the collision in the following way. The system begins asymptotically on the covalent surface. When the particles reach the location of the crossing with the ionic surface, the Landau-Zener formula¹¹ is used to compute the probability of switching to the other surface. As shown in Figure 1, there are two

possible paths to ion-pair formation. The surface crossing may occur on the inward part of the trajectory (the dashed line) or on the outward part (shown by the dotted line). A transfer to the ionic surface will initiate an expansion of the I_2^- bond since I_2^- has a larger equilibrium internuclear distance than I_2 . If this transfer occurs on the incoming trajectory, the resulting I_2^- expansion will yield an effective vertical electron affinity that increases with time. This will increase the radius R at which the second surface crossing is encountered on the outward part of the trajectory. Since the matrix element connecting the two surfaces decreases strongly with increasing R , the probability of a diabatic path through the second crossing may be significantly larger than at the first crossing. These effects have already been thoroughly discussed in the literature.¹⁻⁶

The analytic form of the potential surface we have used differs somewhat from the form used in reference 2. Ours is defined in terms of Figure 2 to be

$$V_{00} = V(R_1) + V(R_2) + v_0(r) \quad (4)$$

$$V_{11} = V(R_1) - \frac{0.5}{R_1} + V(R_2) - \frac{0.5}{R_2} + v_1(r) \quad (5)$$

$v_0(r)$ and $v_1(r)$ are Morse potentials for I_2 and I_2^- respectively. The same Morse parameters were used as in reference 2, namely, $D = 1.54$ eV, $\beta = 1.87 \text{ \AA}^{-1}$, and $r_e = 2.67 \text{ \AA}$ for I_2 , and $D' = 1.02$ eV, $\beta' = 1.23 \text{ \AA}^{-1}$, and $r_e' = 3.20 \text{ \AA}$ for I_2^- . $V(R_1)$ is a repulsive term of the Born-Mayer form,¹²

$$V(R_1) = A e^{-BR_1} \quad (6)$$

where, following reference 2, we initially use $A = 6.4 \times 10^4$ eV and $B = 4.762 \text{ \AA}^{-1}$. Note that for simplicity the same constants A and B are used here for the ionic and covalent terms. The potentials we use are much simpler than those of reference 2. Since ab initio calculations are not available, we choose to use potentials with as few adjustable parameters as possible.

The potential surfaces defined by Eqs. (4) and (5) do not reflect the multiplicity of states arising from the inner shell vacancy in Ar^* . Our simplified model is equivalent to assuming that all of the covalent surfaces are degenerate, and that all of the ionic surfaces are degenerate. This assumption appears reasonable at large values of R, where the surfaces cross. In this region we expect no inner shell rearrangement processes. The core electrons should have only a minor influence on the potential shapes and coupling matrix elements. This fact is indeed the major reason for the strong analogy to alkali reactions and the justification for our use of the single surface crossing and the coupling matrix element angular dependence¹³ ($\cos\alpha$ in Eq. (7) below) that are appropriate to alkali systems. The inner shell vacancy in Ar^* would, however, be expected to influence surface parameters at much smaller R values and thereby could affect the shape of the differential cross sections. We will return to this point later.

We use the same form for the coupling matrix element as in reference 2:

$$V_{12}(R, r, \theta) = c_1 [I + EA(r)]^{\frac{1}{2}} R^* e^{-c_2 R^*} \cos \alpha \quad (7)$$

$$\text{where } R^* = \frac{R}{\sqrt{2}} (I^{\frac{1}{2}} + EA(r)^{\frac{1}{2}}). \quad (8)$$

I is the ionization potential of the projectile and $EA(r)$ is the vertical electron affinity of the molecule as a function of the separation r .

(c_1 in eV; I and EA in a.u.; R in Å; c_2 in Å⁻¹). Note that the diagonal terms V_{00} and V_{11} are orientation-dependent because they are defined in terms of R_1 and R_2 . Note also that the angular dependence of V_{12} forces it to be zero at the angles required by symmetry.¹³ Initially the constants $c_1 = 0.28$ eV and $c_2 = 0.65$ Å⁻¹ were used² for both reaction (1) and reaction (2).

For each orientation of the target (in a space-fixed frame), we wish to calculate the two branches of the classical deflection function. These two branches give the scattering angle as a function of impact parameter for trajectories in which the surface crossing occurs on the inward or outward part of the trajectory. (If the crossing occurs twice, or not at all, ion-pair formation does not occur and the trajectory is not counted.) For each impact parameter, the scattering angles are therefore calculated for two sequences of events. In both cases, the I_2 molecule begins at rest on the neutral potential curve $v_0(r)$ at the equilibrium distance r_e , and the projectile follows a straight-line path with constant velocity throughout the collision. For the ionic

branch of the deflection function, the system is assumed to switch to the ionic potential at the first crossing. Then the I_2^- molecules begin to move classically on the potential $v_1(r)$, beginning at rest at $r = r_e(I_2)$. The location of the second crossing is determined numerically by monitoring the oscillatory motion of the target and the rectilinear motion of the projectile. For the covalent branch of the deflection function, the molecules do not begin to vibrate until the crossing is encountered a second time, so that the first and second crossings occur at the same intermolecular separation R . For both branches of the deflection function, the orientation angle α is computed at both crossings. The orientation influences the transition probability through the factor $\cos \alpha$ in Eq. (7).

The preceding discussion shows how the appropriate potential is determined at each point along a given trajectory. The scattering angle is then determined by integrating the cumulative momentum transfer perpendicular to the rectilinear motion, according to standard formulas¹⁴ of classical perturbation theory. The deflection is easily calculated analytically because the functions in equations (4) and (5) are written as sums of two-body potentials.

In order to obtain the cross section, it is also necessary to calculate the probability that the system will follow a given trajectory. This is done using the Landau-Zener formula.¹⁵ The total probability

for a given sequence of surface crossings or avoided crossings is the product of the probabilities for each event separately. This is easily calculated once the locations of the two crossing points are known. The result for the cross section (for a particular orientation of the molecule) can be summarized in the following formula:

$$\frac{d\sigma}{d\Omega} \sin \theta = \sum_j \frac{2\pi b_j p^{\text{ion}}(b_j)}{|d\theta^{\text{ion}}/db|} + \sum_{j'} \frac{2\pi b_{j'} p^{\text{cov}}(b_{j'})}{|d\theta^{\text{cov}}/db|} \quad (9)$$

$p^{\text{ion}}(p^{\text{cov}})$ is the overall probability of following an ionic (covalent) trajectory for a particular impact parameter b . The sums are understood to be over all impact parameters that lead to the scattering angles θ or $-\theta$. Although eq. (9) presents the formal definition of the cross section, we found it useful in practice to use a conventional histogram procedure.

B. The Penning Ionization Channel.

1. Estimating $\Gamma(R)$ for molecular systems.

$\Gamma(R)/\lambda$ is the rate at which particles are lost from an initial channel into the ionization channel via the reaction (3). Γ is given by^{16,17}

$$\Gamma = 2\pi\rho |H_{fi}|^2 \quad (10)$$

$$= 2\pi\rho |\langle \psi_{\text{final}} | H | \psi_{\text{initial}} \rangle|^2 \quad (11)$$

where H is the Hamiltonian, ψ_{initial} is the initial bound state wave function ($\text{Ar}^* + \text{I}_2$), ψ_{final} is the continuum configuration ($\text{Ar} + \text{I}_2^+ + e^-$) and ρ

is the density of continuum states. If the continuum wave function is normalized to unit amplitude asymptotically, then

$$2\pi\rho = 4/k \quad (12)$$

where the kinetic energy of the ejected electron is, in atomic units,
 $E = 1/2 k^2$.

Miller and Morgner¹⁰ have suggested that the matrix element H_{fi} can be written as the product of an overlap factor and a charge exchange factor. Specializing to our case, $Ar^* + I_2$, this would be the product

$$H_{fi} \cong S_{fi} \times H_{fi}^{(o)} \quad (13)$$

where S_{fi} is the overlap between the valence electron orbital on Ar^* and the final state continuum orbital, and $H_{fi}^{(o)}$ is the matrix element for the one-electron process



Miller and Morgner¹⁰ pointed out that $H_{fi}^{(o)}$ can be estimated using the semi-empirical correlation formula of Olson et al.:¹⁸

$$|H_{fi}^{(o)}| \cong GR e^{-R/C} \quad (15)$$

where R is the internuclear separation in a.u., and

$$1/C = \frac{1}{\sqrt{2}} [I_{I_2}^{1/2} + I_{Ar}^{1/2}] \quad (16)$$

$$G = (I_{I_2} I_{Ar})^{1/2}/C \quad (17)$$

where I_{I_2} and I_{Ar} are the ionization potentials of I_2 and Ar in a.u.,

respectively. $|H_{fi}|$ is then given also in a.u.

Based on past experience¹⁹ calculating continuum overlap factors S_{fi} , we have simplified the Miller-Morgner formula by setting $S_{fi} \approx 1$. This approximation enables us to evaluate H_{fi} without numerical integration. Furthermore, since the potential surfaces are not in general known, we calculate the density of states $2\pi\rho$ from the energy of the ejected electron as $R \rightarrow \infty$. This information is available from spectroscopic data.

Miller and Morgner¹⁰ estimate that their formula is reliable within a factor of three to five. We expect that our additional approximations will degrade the accuracy somewhat, but the result should certainly still be a reasonable order-of-magnitude estimate.

2. Ionization Probability as a Function of Impact Parameter.

The autoionization rate obtained in the previous section has the form $\Gamma(R) \propto R^2 e^{-\lambda R}$. However, we have found that over the important range of R probed in the collisions, the numerical values of Γ can be well fit (~10%) by the simpler form

$$\Gamma(R) = a_1 e^{-\frac{a}{2}R} \quad (18)$$

This is the form of Γ that has been assumed in many previous semi-empirical studies.^{20,21}

We have found that for a Γ of the form of Eq. (18), a very simple formula can be obtained, in the perturbation limit, for the ionization probability as a function of impact parameter. Since

the translational motion is already treated using classical perturbation theory, a perturbation assumption for the continuum coupling is consistent with the rest of the model.

Let b be the impact parameter. Then the survival probability $P(b)$ that ionization does not occur on a trajectory of impact parameter b is

$$P(b) = \exp[-2F(b)] \quad (19)$$

where in the perturbation limit

$$F(b) = \int_b^{\infty} \frac{\Gamma(R) dR}{\hbar v_0 \sqrt{1 - (b^2/R^2)}} \quad (20)$$

and v_0 is the incident velocity.

Substituting Eq. (18) into Eq. (20), integrating by parts, and substituting $x = R/b$, we obtain

$$F(b) = \frac{a_1 a_2 b^2}{\hbar v_0} \int_1^{\infty} \frac{e^{-a_2 b x}}{\sqrt{x^2 - 1}} dx \quad (21)$$

The integral can be represented in terms of the modified Bessel function K_1 . Then

$$F(b) = \frac{a_1 b}{\hbar v_0} K_1(a_2 b) \quad (22)$$

Further simplification is possible because of the relation

$$x K_1(x) \approx 2.076 e^{-0.932 x} \quad (23)$$

which is valid to about 10% for $2 \leq x \leq 12$. The final result is

$$F(b) \approx \frac{2.076 a_1}{a_2 \hbar v_0} e^{-0.932 a_2 b} \quad (24)$$

Formulas (19) and (24) may now be incorporated into the model in the following way. For each orientation, a deflection function is calculated that gives the angular scattering as a function of impact parameter. When the cross section is calculated from a particular branch of the deflection function, a factor is first included to represent the probability that the particles follow the correct sequence of curve crossings. The result is then multiplied by $P(b)$, which gives the probability that the trajectory is completed without loss to ionization.

III RESULTS AND DISCUSSION

A. $K + I_2$

This reaction has already been treated in detail.²⁻⁴ Here we demonstrate that the use of the potentials defined in Section II-A leads also to satisfactory agreement with experiment. In Figure 3, we compare the calculated and experimental values at a lab energy (E_0) of 60 eV. The agreement is not surprising since our potentials are nearly the same as those fitted to the data in reference 2. The major difference is that we have neglected the small van der Waals term.

B. $Ar^* + I_2$: General Approach

Gillen et al.¹ pointed out that their results for $Ar^* + I_2$ were similar to those of Aten et al.² for $K + I_2$. The important differences are that the covalent peak is relatively somewhat smaller for $Ar^* + I_2$ than for $K + I_2$ and that the rainbow in the ionic peak occurs at smaller angles. The first difference could be caused by the continuum coupling in the metastable system or by differences in the potentials and charge exchange matrix elements. The second difference should be associated with a difference in the shape of the potential surfaces.

In this and the following subsections we describe our quantitative calculations to investigate possible causes for the experimental differences. With only a qualitative knowledge of the $Ar^* + I_2$ potential surfaces, we do not expect to determine uniquely the coupling parameters

in this system. Hence, our approach to $\text{Ar}^* + \text{I}_2$ ion-pair formation calculations is to start with the $\text{K} + \text{I}_2$ parameters and determine the changes in the distributions caused by individually altering the continuum width ($\bar{\Gamma} = 0$ initially), the surface coupling parameters, and the interaction potentials. The results should yield insight into the possible causes of the differences observed between $\text{Ar}^* + \text{I}_2$ and $\text{K} + \text{I}_2$ in the ion-pair channel.

We initially performed trial calculations for $\text{Ar}^* + \text{I}_2$ assuming $\bar{\Gamma} = 0$, and using the same potential parameters as for $\text{K} + \text{I}_2$. The crossing point differs slightly for this system because the ionization potential of Ar^* is slightly smaller than that for K . This change increases R_c somewhat, and thereby decreases V_{12} slightly, but the effect on the calculations was quite small. The calculated peak ratios and the position of the rainbow angle were essentially the same as those calculated for $\text{K} + \text{I}_2$, and these values did not agree with the data for $\text{Ar}^* + \text{I}_2$.

C. $\text{Ar}^* + \text{I}_2$: The Continuum Channel.

We then examined the effect of including continuum coupling. It should be noted that $\bar{\Gamma}(R)$ is assumed to affect only the covalent potential. This is consistent with the conclusions of Hultsch et al.²² on similar systems. One argues that Penning ionization of the covalent electronic state is initiated by a one-electron process, namely the "exchange" process, in which an electron from the ground state atom jumps into the

hole of the excited atom. There is then a large overlap between the valence electron of the excited atom and the continuum orbital. In contrast for a system on the $\text{Ar}^+ + \text{I}_2^-$ surface, continuum coupling necessitates a simultaneous two-electron rearrangement; such a process would be expected to have a much lower probability.

For the ground electronic state of I_2^+ , which is 9.3 eV above I_2 , we follow the prescription of Section II-B and obtain (for Γ and R in atomic units)

$$\Gamma(R) = 1.752 R^2 e^{-1.902R} \quad (25)$$

For R in the range 4 - 12 a_0 , this is well fit by the form

$$\Gamma_0(R) \cong 11.16 e^{-1.614R} \text{ a.u.} \quad (26)$$

We performed calculations using this form of $\Gamma(R)$ and keeping the other potential parameters the same. The result is that the continuum coupling is not large enough to cause a significant effect on the ion-pair distributions.

The charge transfer matrix element estimated from Eq. (15) is a one-electron matrix element. In fact $\Gamma(R)$ should be larger than $\Gamma_0(R)$ to account for the two equivalent electrons in the $2\pi_{1/2,g}$ orbital. Moreover, the I_2 molecule has a valence configuration $(\sigma_g 5p)^2 (\pi_{1/2,u} 5p)^2 (\pi_{3/2,u} 5p)^2 (\pi_{1/2,g} 5p)^2 (\pi_{3/2,g} 5p)^2$, and these ten electrons have vertical ionization potentials²³ between 9.3 and 13.0 eV. In the spirit of our

AD-A088 746

SRI INTERNATIONAL MENLO PARK CA
THEORETICAL STUDY OF STATE-TO-STATE COLLISIONS.(U)

F/G 20/8

JUN 80 A P HICKMAN, R P SAXON

F44620-75-C-0073

UNCLASSIFIED

SRI-MP-80-72

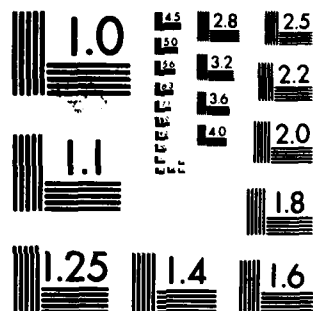
AFOSR-TR-80-0682

NL

2

11

END
DATE
FILMED
10 80
DTIC



MICROCOPY RESOLUTION TEST CHART
NATIONAL BUREAU OF STANDARDS 1963 A

one-electron estimate of Γ_0 , we should also calculate approximate continuum coupling widths for the other electrons.

Although the ionization potential for electrons in the lowest two of these orbitals is larger than the Ar^* excitation energy, Miller and Morgner¹⁰ have shown that the electronic energy transfer to a pseudo-continuum Rydberg state,



(core-excited in this case) can be treated in an equivalent way to a true continuum interaction. The details of the formula are slightly different; however, the calculated coupling widths are found to be quite similar to those for states whose ionization potentials are lower than the excitation energy of the incoming state. Assuming the contributions for all ten electrons can be added (a reasonable first approximation), we obtain a resultant $\Gamma(R)$ that is 10-15 times larger than $\Gamma_0(R)$ for R values between 5 and 11 a.u.

The effects of various coupling functions $\Gamma(R)$ on the calculated angular distribution for reaction (1) at 28 eV are shown in Figure 4. Continuum effects are generally more pronounced at lower energies, and $E_0 = 28$ eV is the lowest energy studied. Clearly $\Gamma = 10 \Gamma_0$, which approximates the summed ten electron continuum coupling estimated above, yields a noticeable depletion of the covalent peak. However, $\Gamma > 100 \Gamma_0$ seems required before the intensity ratios of the covalent and ionic

peaks are in reasonable agreement with experiment. Since our approximate estimates of Γ are relatively crude, it is possible that Γ is indeed an order of magnitude larger than estimated. Hence, the continuum coupling effect could make some contribution to the attenuation of the covalent peak in reaction (1). However, the larger Γ values ($100 \Gamma_0$, $1000 \Gamma_0$) give covalent peaks that are strongly attenuated at low τ values; the angular positions of the calculated peaks then disagree considerably with the data.

D. $\text{Ar}^* + \text{I}_2$: Sensitivity to the Coupling Matrix Element V_{12} .

Another possible cause for the smaller covalent peak in $\text{Ar}^* + \text{I}_2$ could be a larger coupling matrix element V_{12} . We have performed calculations in which $\Gamma = 0$ and the constant c_1 of V_{12} is varied [see Eq. (7)]. We find that a significant change in V_{12} from the value for $\text{K} + \text{I}_2$ is needed to cause the desired change in $\text{Ar}^* + \text{I}_2$ peak ratios. Figure 5 shows the experimental angular distribution at $E_0 = 51$ eV, compared with three calculations assuming V_{12} multiplied by factors of 1.0, 2.5, and 5.0 relative to $\text{K} + \text{I}_2$. Even though the peak ratios are accurately matched by scaling V_{12} by approximately 2.5, we feel that this is an unreasonable change considering the expected similarities between K and Ar^* . Although the potential surfaces for the two reactions have quite different symmetries, these differences are associated with the symmetry of the Ar^* core. At the very large crossing radius (~ 5.7 Å) between the ionic

and covalent surfaces, the properties of the core should play a minor role in the electron transfer process and the outer Ar^* electron should behave like a 4s electron in K.

E. $\text{Ar}^* + \text{I}_2$: Sensitivity to V_{22} .

It is obvious from Figure 5 that the calculated rainbow angle is not in good agreement with the experimental data. None of the modifications detailed above has altered the calculated rainbow position. Since its position is most sensitive to the well depth in the ionic channel, we investigated modifications to the potential parameters necessary for achieving a match to the experimental rainbow angle. In our model, the well depth is controlled by the choice of the parameters A and B in Eq. (6). We found that varying these parameters to decrease the well depth caused the rainbow to shift to smaller angles, as expected. Another effect of this change was a reduction in the size of the covalent peak relative to the ionic peak. Figure 6 shows the effect of changes in the potential parameters upon the ion-pair distributions. The modification that gave a reasonable fit to the ionic rainbow angle corresponds to an $\text{Ar}^+ - \text{I}_2^-$ "well-depth" that is ~ 0.5 eV shallower than that of $\text{K}^+ + \text{I}_2^-$ (at the same I-I internuclear separation).

For comparison, there are good ab initio calculations for the diatomic potentials in ArF , KrF , and the Xe halides.²⁴ For each of these systems the well depths of the various ion-pair states are

between 0.3 eV and 0.7 eV shallower than those of the analogous alkali halide molecule. With spin-orbit coupling included, the three ion-pair states calculated for each rare-gas halide pair differ by less than ~ 0.2 eV in well depth and 0.1 \AA in R_e from each other. If a similar result obtained for the triatomic systems, our method of treating the $\text{Ar}^* + \text{I}_2$ system by a single (average) ion-pair surface intersecting a single covalent surface would be a reasonable approximation to the average scattering on the relevant surfaces and our resultant 0.5 eV difference in $\text{Ar}^+ - \text{I}_2^-$ and $\text{K}^+ - \text{I}_2^-$ well depths would appear to be reasonable.

F. $\text{Ar}^* + \text{I}_2$: Conclusions.

Our calculations clearly indicate that the ion-pair angular distributions for reaction (1) depend quite sensitively on the shapes of the interaction potentials, the surface coupling matrix elements, and the amount of depletion from competing continuum coupling and excitation transfer channels. With only crude model potentials and order-of-magnitude estimates for the continuum coupling and excitation transfer effects, it does not seem justified to vary parameters to achieve a fit to the data that would be both model-dependent and non-unique. However, an estimate of the probable causes for the differences from reaction (1) can be useful in suggesting directions for further experimental or theoretical effort on this system.

The shift of the ionic rainbow for reaction (1), to lower τ values than that for reaction (2), seems to be consistent with a shallower well in the $\text{Ar}^+ + \text{I}_2^-$ interaction (see Figure 6). This change also lowers the magnitude of the covalent peak relative to the ionic peak. In fact all other modifications combined would only need to lower the covalent peak by an additional 30-40% to achieve a good agreement with the experimental data at $E_0 = 51 \text{ eV}$.²⁵

Combined with the change in the ionic potential described in Section E, an increase of c_1 by ~40% over the $\text{K} + \text{I}_2$ value (0.28 eV) would achieve a reasonable match to the experimental data. However, such a change in V_{12} still seems rather large. As evidence for this assertion, we note that Hubers et al.²⁶ present a reduced matrix element formula that is slightly modified from Eq. (7) and correlates with all alkali-halogen systems to an accuracy of better than 10%. The modification of the $\text{Ar}^* + \text{I}_2$ matrix element postulated here would deviate by 40% from the prediction²⁶ based on the alkali data and would then suggest some real differences of Ar^* from alkali-like properties at distances of $R_c \approx 5.7 \text{ \AA}$. It is difficult to understand such a large effect at that distance caused by a vacancy in the ion core.

Alternatively, a continuum coupling width of $\sim 40 \Gamma_0$ could be combined with the shallower ionic potential to match the peak ratios adequately. This width is somewhat larger than the rough estimate ($10\text{-}15 \Gamma_0$) based on the Miller-Morgner¹⁰ arguments, and the attenuated covalent peak would

be located at larger τ values than the data would allow. Yet our estimate of τ is subject to considerable uncertainty and could be significantly in error. Also, the covalent peak position and shape are sensitively dependent on the potential functions used. This has been demonstrated⁴ in $K + Br_2$ by a comparison of calculations on diabatic and adiabatic surfaces. Hence, continuum coupling (3) and excitation transfer (27) reactions involving the ten valence I_2 electrons could be responsible for all or part of the remaining 30-40% depletion of the covalent peak.

Finally, we note that making the potentials more repulsive tends to decrease the size of the covalent peak relative to the ionic peak. For simplicity, we have constrained our calculations so that the repulsive Born-Mayer terms are identical on the ionic and covalent surfaces. Although this is a reasonable first approximation, one could decrease the covalent peak by relaxing this constraint and allowing more repulsion in the covalent potential. If such a difference were responsible for the smaller covalent peak in (1) relative to (2), it would necessarily imply differences between the two systems in the repulsive region. This is easier to accept than large differences (40%) in the coupling matrix elements at the much larger distances associated with the surface crossings.

IV SUMMARY

The small differences between the differential cross sections for ion-pair formation in the $\text{Ar}^* + \text{I}_2$ and $\text{K} + \text{I}_2$ system can be explained, in part, by a more repulsive wall in the ionic $\text{Ar}^+ + \text{I}_2^-$ surface relative to $\text{K}^+ + \text{I}_2^-$. This yields a smaller ionic well depth (by ~ 0.5 eV at r_e of I_2) and a correspondingly smaller ionic rainbow angle that is in agreement with the data. If the covalent surfaces $\text{Ar}^* + \text{I}_2$ and $\text{K} + \text{I}_2$ have repulsive terms similar to those on their ionic counterparts, the calculated ratio for the intensity of the covalent peak to the ionic peak in reaction (1) is too large by a factor of ~ 1.4 .

This ratio can be improved by one or more of the following: a relative increase in the repulsion on the $\text{Ar}^* + \text{I}_2$ covalent surface; a depletion of the covalent peak by competing Penning (3) and excitation transfer (27) reactions; and an increase in the coupling matrix element at the surface crossing between the ionic and covalent surfaces. The third possibility seems least likely since it requires effects from the Ar^* core vacancy to be important at large R (~ 5.7 Å).

Since the potential surfaces have only been estimated in a crude way and since the continuum coupling width is only known very approximately, we feel that no claim to a unique fit can be made. Continuum coupling and excitation transfer processes may indeed cause observable, but small, depletions of the covalent peak in the ion-pair process (1).

ACKNOWLEDGEMENTS

This work was supported by the Office of Naval Research and by the Air Force Office of Scientific Research under Contract FF44620-75-C-0073. The authors are especially grateful to A. Kleyn and J. Los for providing their computer program and for assisting in its implementation. Helpful comments from D. L. Huestis, A. Kleyn, H. Morgner, and A. Niehaus are also gratefully acknowledged.

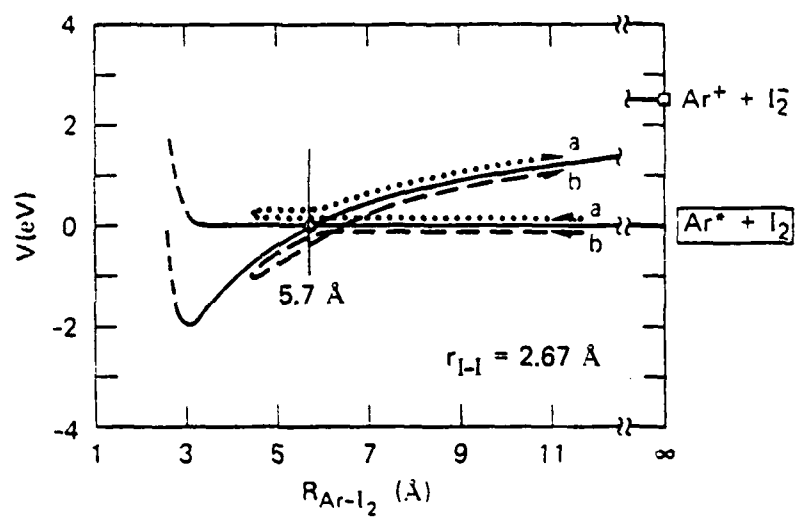
REFERENCES

1. K. T. Gillen, T. D. Gaily and D. C. Lorents, Chem. Phys. Lett. 57, 192 (1978).
2. J. A. Aten, G.E.H. Lanting and J. Los, Chem. Phys. 19, 241 (1977).
3. J. A. Aten, G.E.H. Lanting, and J. Los, Chem. Phys. 22, 333 (1977).
4. J. A. Aten and J. Los, Chem. Phys. 25, 47 (1977).
5. J. Los, in: Proceedings of the Tenth International Conference on the Physics of Electronic and Atomic Collisions, Invited Papers and Progress Reports", ed. G. Watel (North Holland, Amsterdam, 1978) p. 617.
6. J. Los and A. W. Kleyn, in: Alkali Halide Vapors, eds. P. Davidovits and D. L. McFadden (Academic Press, New York, 1979) p. 275.
7. S. Wexler and E. K. Parks, Ann. Rev. Phys. Chem. 30, 179 (1979).
8. J. C. Tully and R. K. Preston, J. Chem. Phys. 55, 562 (1971).
9. R. K. Preston and R. J. Cross, J. Chem. Phys. 59, 3616 (1973).
10. W. H. Miller and H. Morgner, J. Chem. Phys. 67, 4923 (1977).
11. N. F. Mott and H.S.W. Massey, The Theory of Atomic Collisions, 3rd Edition (Clarendon Press, Oxford, 1965), p. 353.
12. M. Born and J. E. Mayer, Z. Physik 75, 1 (1932).
13. E. A. Gislason and J. G. Sachs, J. Chem. Phys. 62, 2678 (1975).
14. L. D. Landau and E. M. Lifshitz, Mechanics, 2nd Edition (Pergamon Press, Oxford, 1969), p. 55-56.
15. L. D. Landau, J. Phys. (USSR) 2, 46 (1932); C. Zener, Proc. Roy. Soc. (London) A137, 696 (1932).
16. W. H. Miller, Chem. Phys. Lett. 4, 627 (1970).
17. W. H. Miller, J. Chem. Phys. 52, 3563 (1970).

18. R. E. Olson, F. T. Smith, and E. Bauer, Appl. Optics 10, 1848 (1971).
19. A. P. Hickman, A. D. Isaacson, and W. H. Miller, J. Chem. Phys. 66, 1483 (1977).
20. A. P. Hickman and H. Morgner, J. Phys. B 9, 1765 (1976).
21. Z. F. Wang, A. P. Hickman, K. Shobatake, and Y. T. Lee, J. Chem. Phys. 65, 1250 (1976).
22. W. Hultzsich, W. Kronast, A. Niehaus, and M. W. Ruf, J. Phys. B 12, 1821 (1979).
23. D. C. Frost, C. A. McDowell and D. A. Vroom, J. Chem. Phys. 46, 4255 (1967); A. B. Cornford, D. C. Frost, C. A. McDowell, J. L. Ragle, and I. A. Strenhouse, J. Chem. Phys. 54, 2651 (1971).
24. T. H. Dunning, Jr. and P. J. Hay, J. Chem. Phys. 69, 134 (1978); P. J. Hay and T. J. Dunning, Jr., J. Chem. Phys. 69, 2209 (1978).
25. That experiment is considered the most reliable, since the signal levels were much smaller at lower energies ($E_0 = 28$ eV) and the angular resolution was much lower at higher energies.
26. M. M. Hubers, A. W. Kleyn, and J. Los, Chem. Phys. 17, 303 (1976).

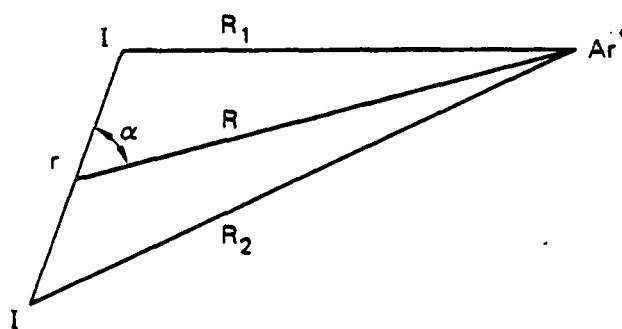
FIGURE CAPTIONS

1. Two possible paths a and b to ion pair production are schematically indicated. The potential curves represent cuts of the $\text{Ar}^* + \text{I}_2$ and $\text{Ar}^+ + \text{I}_2^-$ surfaces at a fixed I_2 separation.
2. Illustration of the coordinate system used to define the potential functions.
3. Comparison of previous calculations and experimental data (Ref. 2) on the system $\text{K} + \text{I}_2$ with the present calculation, which uses slightly different interaction potentials.
4. Calculation of the differential cross section for ion pair formation in $\text{Ar}^* + \text{I}_2$ compared with the data of Ref. 1. The effect of different autoionization rates $\Gamma(R)$ in the covalent channel is illustrated. Γ_0 is the function estimated using the method discussed in Section II-B-1, and given by Eq. (26). Successively larger values of $\Gamma(R)$ reduce the covalent peak by larger fractions.
5. Calculation of the differential cross section for ion pair formation in $\text{Ar}^* + \text{I}_2$ compared with the data of Ref. 1. The effect of different coupling matrix elements V_{12} is illustrated. $\Gamma(R)$ is set to zero in all cases. V_{12}^0 is the form given by Eq. (7) with $c_1 = 0.28$ eV and $c_2 = 0.65 \text{ \AA}^{-1}$, the same parameters used in Ref. 1 for $\text{K} + \text{I}_2$. The scaled values of V_{12} correspond to changing c_1 to 0.7 eV and 1.4 eV.
6. Calculation of the differential cross section for ion pair formation in $\text{Ar}^* + \text{I}_2$ compared with the data of Ref. 1. The potential parameters, defined in Eqns. (4) - (6), are $A = 6.4 \times 10^4$ eV and $B = 4.762 \text{ \AA}^{-1}$ for the original well, and $A = 1.35 \times 10^4$ eV and $B = 3.781 \text{ \AA}^{-1}$ for the shallower well.



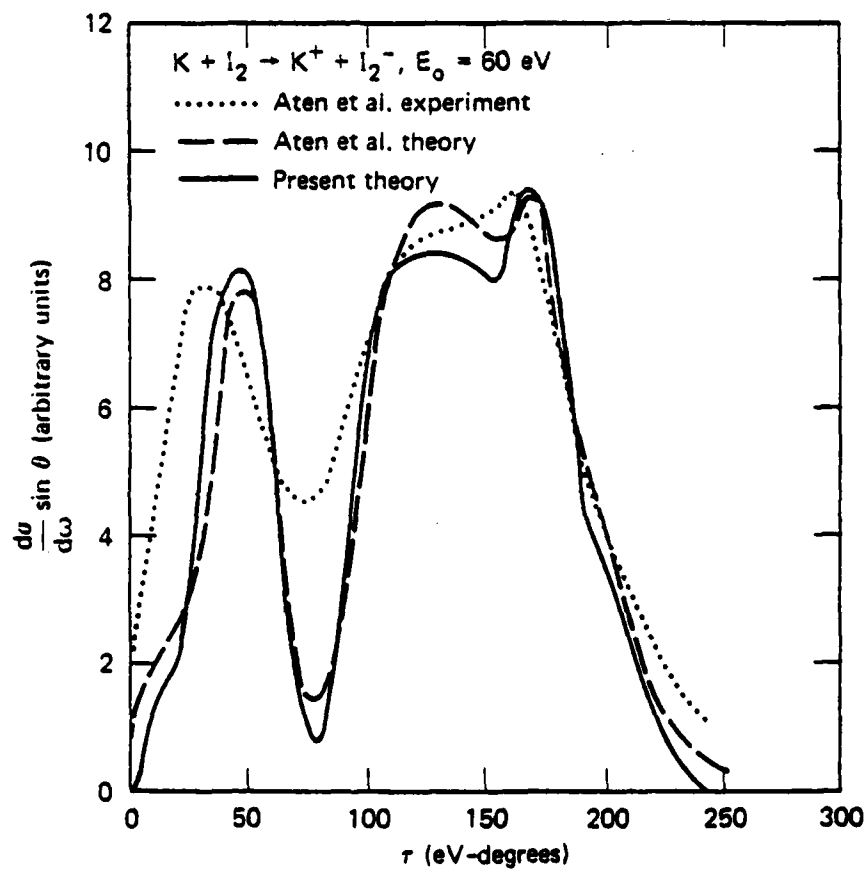
SA-5389-2A

Figure 1



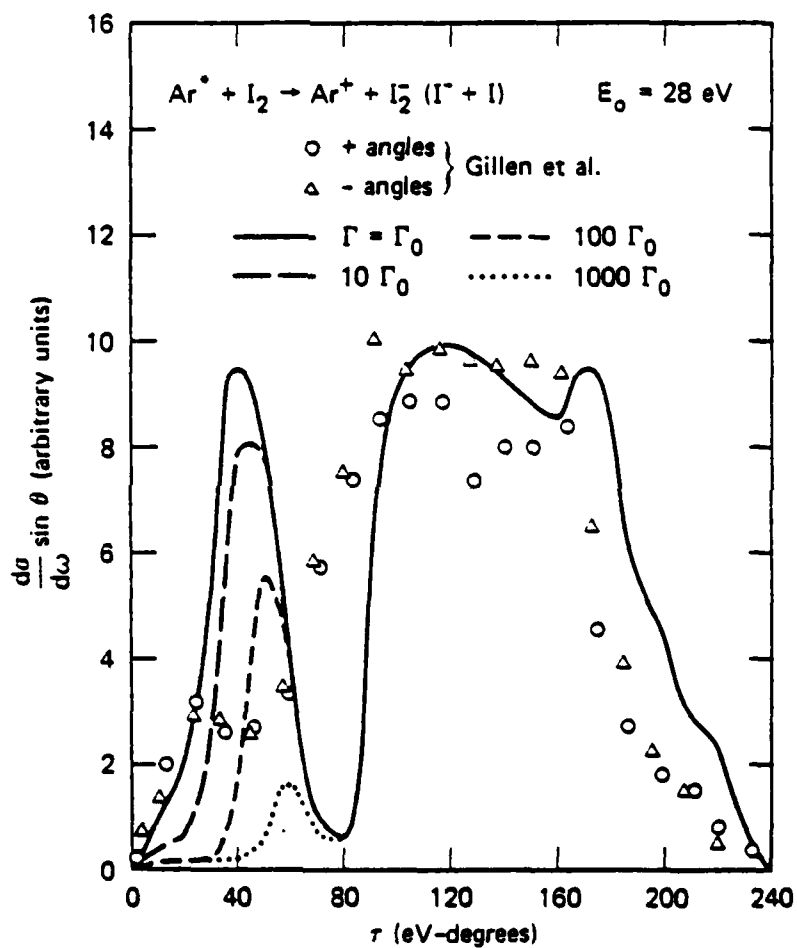
SA-5389-18R

Figure 2



SA-5389-21

Figure 3



SA-5389-22R

Figure 4

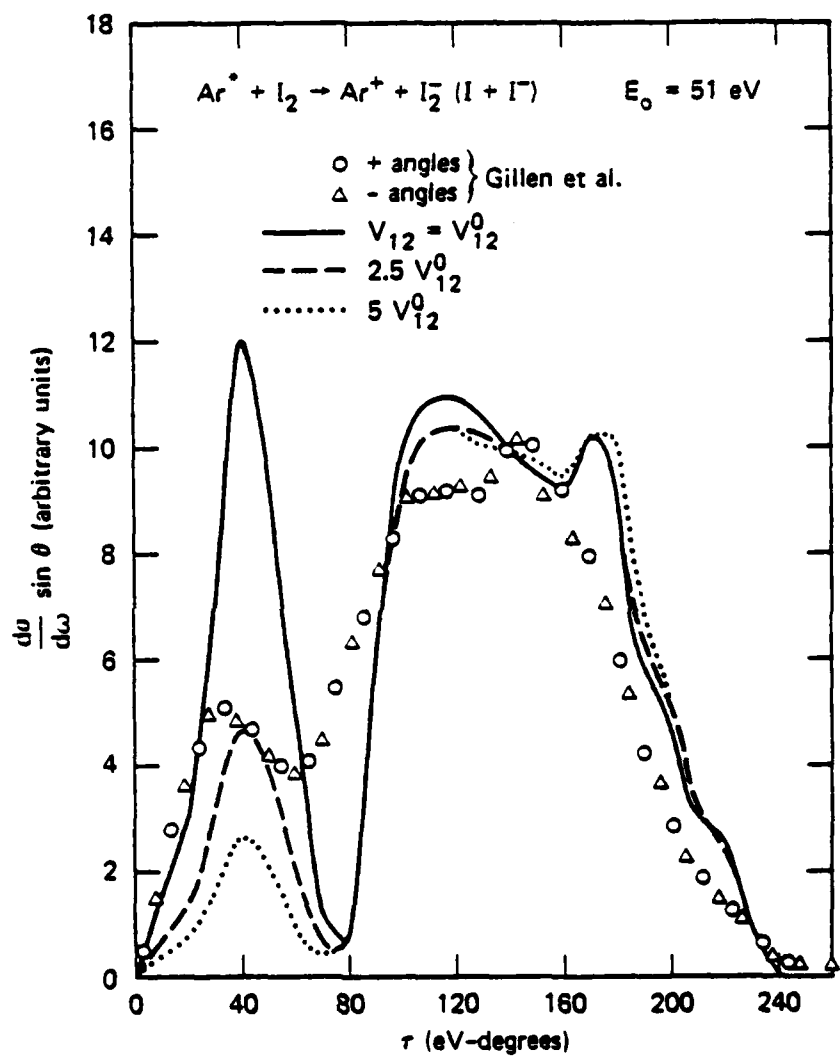
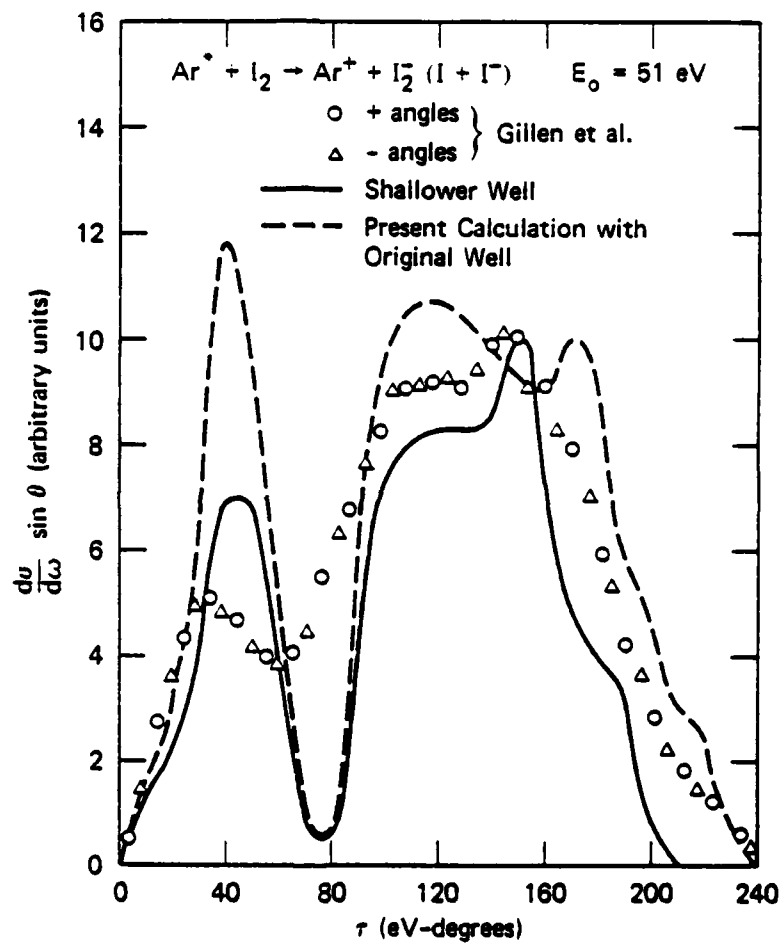


Figure 5



SA-5389-25

Figure 6

APPENDIX D

MODEL FOR FAST, NON-ADIABATIC COLLISIONS BETWEEN ALKALI ATOMS AND DIATOMIC MOLECULES

A. P. Hickman
Molecular Physics Laboratory
SRI International
Menlo Park, CA 94025

ABSTRACT

Equations for collisions involving two potential surfaces are presented in the impact parameter approximation. In this approximation, a rectilinear classical trajectory is assumed for the translational motion, leading to a time-dependent Schroedinger's equation for the remaining degrees of freedom. Model potentials are considered for collisions of alkali atoms with diatomic molecules that lead to a particularly simple form of the final equations.

Using the Magnus approximation, these equations are solved for parameters chosen to model the process $\text{Cs} + \text{O}_2 \rightarrow \text{Cs}^+ + \text{O}_2^-$, and total cross sections for ion-pair formation are obtained as a function of energy. The results exhibit oscillations that correspond qualitatively to those seen in recent measurements. In addition, the model predicts that the oscillations will become less pronounced as the initial vibrational level of O_2 is increased.

MP 30-67

I. INTRODUCTION

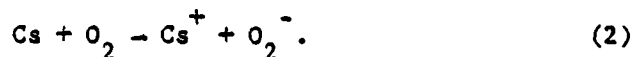
In this paper we consider the process of ion-pair formation in collisions between alkali atoms and diatomic molecules:



An important feature of this process is that two electronic potential surfaces are involved, the location of whose crossing depends both on the vibrational and translational coordinates. Considerable work has been done to analyze experimental data in terms of a perturbative, classical trajectory, surface-hopping model.¹⁻³ The agreement is satisfactory for many systems. However, there has been a tendency to try to improve the basic model by introducing various ad hoc modifications. Here we will attempt to treat the process using a more systematic theory.

Our approach is based on the semiclassical impact parameter approximation.⁴ We choose a model form for the two potential surfaces that is consistent with previous work,^{5,6} and also leads to a particularly simple form of the final equations of motion. We assume that the translational motion is a straight line trajectory with constant velocity, and then focus on the quantum mechanical evolution of the remaining degrees of freedom under the resulting time-dependent Hamiltonian. An approximate, unitary S matrix is found using the Magnus approximation.⁷

In Section II we present the equations of motion in the impact parameter approximation for collisions involving two potential surfaces that are functions of vibrational and translational coordinates. A matrix notion is used that highlights the manner in which the second potential surface affects the motion. It is shown how rotational degrees of freedom may be treated using the sudden approximation. In Section III results are obtained for potential surfaces chosen to model the specific system



Total cross sections for ion-pair formation as a function of energy are calculated. Because of the model nature of the potential surface, and the perturbation solution of the equations of motion, the results are not expected to be quantitative. However, the results are in qualitative agreement with recent experiments.⁸ Concluding remarks are given in Section IV.

II. THEORY

A. General Equations

We first develop the equations of the impact parameter approximation for the case of two electronic potential surfaces that depend on a translational coordinate R and a vibrational coordinate r . In the next section we shall derive the form taken by these equations for our particular model potential, and show how the rotational motion may be included using the sudden approximation.

Let us take the matrix elements of the total Hamiltonian of the system in a basis of two (diabatic) electronic functions. We will assume that the resulting operator has the following form:

$$H = (T_R + T_r) \underline{1} + \begin{bmatrix} v_0(r) + V_0(R) & 0 \\ 0 & v_1(r) + V_1(R) \end{bmatrix} + \begin{bmatrix} W_{00}(R, r) & W_{01}(R, r) \\ W_{01}(R, r) & W_{11}(R, r) \end{bmatrix} \quad (3)$$

Note that we have isolated the separable part of the diagonal potential matrix elements. The translational and vibrational coordinates are R and r , respectively. We now assume that the translational motion is given by

$$R(t) = \left[b^2 + (vt)^2 \right]^{\frac{1}{2}} \quad (4)$$

where b and v are the impact parameter and relative velocity, respectively.

We can now write the following time-dependent Hamiltonian for the remaining degrees of freedom:

$$\hat{H} = \begin{bmatrix} T_r + v_0(r) + w_0(t) & 0 \\ 0 & T_r + v_1(r) + w_1(t) \end{bmatrix} + \begin{bmatrix} W_{00}(R(t), r) & W_{01}(R(t), r) \\ W_{01}(R(t), r) & W_{11}(R(t), r) \end{bmatrix} \quad (5)$$

where

$$w_i(t) = V_i(R(t)) \quad i = 0, 1 \quad (6)$$

Let us assume that the eigenfunctions ϕ_λ^i and eigenvalues ϵ_λ^i of the target Hamiltonians are known:

$$[T_r + v_i(r)] \phi_\lambda^i = \epsilon_\lambda^i \quad i = 0, 1 \quad (7)$$

Then the time-dependent Schroedinger's equations resulting from the diagonal terms in the first set of brackets in (5) may be solved exactly.

That is,

$$(T_r + v_i(r) + w_i(t)) \psi_\lambda^i(r, t) = \frac{\partial}{\partial t} \psi_\lambda^i(r, t) \quad i = 0, 1 \quad (8)$$

has the exact solution

$$\psi_\lambda^i(r, t) = \phi_\lambda^i(r) \exp \left\{ -i \int_0^t [\epsilon_\lambda^i + w_i(t')] dt' \right\} \quad i = 0, 1 \quad (9)$$

The lower limit of the integral corresponds to an arbitrary phase factor and is chosen for later convenience to be zero.

We now wish to solve

$$H \psi^{\text{total}}(r, t) = i \frac{\partial}{\partial t} \psi^{\text{total}}(r, t) \quad (10)$$

in terms of the following two component expansion:

$$\psi^{\text{total}}(r, t) = \sum_{\mu=1}^N \alpha_{\mu}(t) \begin{bmatrix} \psi_{\mu}^0(r, t) \\ 0 \end{bmatrix} + \sum_{\lambda=1}^N \beta_{\lambda}(t) \begin{bmatrix} 0 \\ \psi_{\lambda}^1(r, t) \end{bmatrix} \quad (11)$$

Substituting (11) with (10) and taking matrix elements in the standard way, we obtain the following set of equations:

$$\begin{bmatrix} \dot{\alpha}_1(t) \\ \vdots \\ \dot{\alpha}_N(t) \\ \dot{\beta}_1(t) \\ \vdots \\ \dot{\beta}_N(t) \end{bmatrix} = -i \begin{bmatrix} \underline{F}(t) & \underline{A}(t) \\ \underline{A}^{\dagger}(t) & \underline{G}(t) \end{bmatrix} \begin{bmatrix} \alpha_1(t) \\ \vdots \\ \alpha_N(t) \\ \beta_1(t) \\ \vdots \\ \beta_N(t) \end{bmatrix} \quad (12)$$

Note that we have used a notation in which the set of $2N$ coupled differential equations is represented in terms of blocks, where each block is an $N \times N$ matrix. The blocks are given as follows:

$$F_{\mu\lambda}(t) = \langle \psi_{\mu}^0(r) | W_{00}(R(t), r) | \psi_{\lambda}^0(r) \rangle \exp \left\{ i \int_0^t [\epsilon_{\mu}^0 - \epsilon_{\lambda}^0] dt' \right\} \quad (13)$$

$$G_{\mu\lambda}(t) = \langle \psi_{\mu}^1(r) | W_{11}(R(t), r) | \psi_{\lambda}^1(r) \rangle \exp \left\{ i \int_0^t [\epsilon_{\mu}^1 - \epsilon_{\lambda}^1] dt' \right\} \quad (14)$$

$$A_{\mu\lambda}(\tau) = \left\langle \phi_{\mu}^0(r) | W_{01}(R(\tau), r) | \phi_{\lambda}^1(r) \right\rangle \exp \left\{ i \int_0^{\tau} \left[\epsilon_{\mu}^0 + w_0(\tau') - \epsilon_{\lambda}^1 - w_1(\tau') \right] d\tau' \right\} \quad (15)$$

A^{\dagger} is the Hermitian conjugate of A:

$$A_{\mu\lambda}^{\dagger}(\tau) = \left\langle \phi_{\lambda}^0(r) | W_{01}(R(\tau), r) | \phi_{\mu}^1(r) \right\rangle \exp \left\{ -i \int_0^{\tau} \left[\epsilon_{\mu}^0 + w_0(\tau') - \epsilon_{\lambda}^1 - w_1(\tau') \right] d\tau' \right\} \quad (16)$$

There will be $2N$ solution vectors, corresponding to the system beginning at $\tau = -\infty$ in each of the possible states $\left\{ \phi_{\mu}^0 \right\}$, $\mu = 1, 2, \dots, N$ and $\left\{ \phi_{\lambda}^1 \right\}$, $\lambda = 1, \dots, N$. If we solve Eq. (12) subject to the initial condition that the solution matrix is the unit matrix at $\tau \rightarrow -\infty$, then the value of the solution at $\tau \rightarrow +\infty$ can be used to find the probability that the system is in each possible final state after the collision. Each element of the solution matrix at $\tau = +\infty$ is, within a phase factor, equal to the corresponding element of the S matrix. This phase factor will be discussed later.

B. Application to a Model System

1. Isotropic Potentials

In this section we will consider the form of Eq. (12) for a particular set of potentials chosen to model collisions of alkali atoms with diatomic molecules. Such systems are characterized by surface crossings at fairly large values of R ($\gg 6a_0$), so that near the crossings fairly simple analytic approximations may be appropriate. We will use analytic potentials similar to those already discussed in previous work:^{5,6}

$$V_0(R) = 0 \quad (17)$$

$$V_1(R) = \Delta E - \frac{1}{R} \quad (18)$$

$$W_{00}(R) = W_{11}(R) = 0 \quad (19)$$

$$W_{01}(R) = c_1 \exp(c_2 R) \quad (20)$$

$$V_i(r) = A_i \left\{ \exp \left[-2\beta_i (r - r_i) \right] - 2 \exp \left[-\beta_i (r - r_i) \right] \right\} \quad (21)$$

These analytic functions model the behavior of the surface at large values of R . The covalent surface is approximately constant, the ionic surface is coulombic, and their asymptotic separation is ΔE . Such potentials are expected to be adequate as long as the major part of the cross section comes from trajectories with large impact parameters. It should be noted that one could add the same repulsive term to V_0 and V_1 without affecting the transition probabilities, since the formulas to be presented here depend only on the difference potential. This modification would allow V_0 and V_1 to be more realistic at small R .

Equations (12)-(21) lead to the following simplifications in Eq. (12). First, the diagonal blocks \underline{F} and \underline{G} vanish entirely because of Eq. (19). These are the terms that lead to vibrationally inelastic scattering on a single surface. Second, the matrix elements of $W_{01}(R(t), r)$ reduce to a function of t times the Franck-Condon factor

$$C_{\mu\lambda} = \langle \phi_{\mu}^0(r) | \phi_{\lambda}^1(r) \rangle \quad (22)$$

because, according to Eq. (20), W_{01} is independent of r . Finally, the integral inside the exponential can be done analytically. The final form of the equations is thus

$$\begin{bmatrix} \dot{\alpha}_1(t) \\ \vdots \\ \dot{\alpha}_N(t) \\ \dot{\beta}_1(t) \\ \vdots \\ \dot{\beta}_N(t) \end{bmatrix} = -i \begin{bmatrix} 0 & -\underline{A}(t) \\ \underline{A}^\dagger(t) & 0 \end{bmatrix} \begin{bmatrix} \alpha_1(t) \\ \vdots \\ \alpha_N(t) \\ \beta_1(t) \\ \vdots \\ \beta_N(t) \end{bmatrix} \quad (23)$$

where

$$A_{\mu\lambda}(t) = C_{\mu\lambda} w_{01}(t) \exp \{if(t)\} \quad (24)$$

$$w_{01}(t) = c_1 \exp \left\{ -c_2 \left[b^2 + (vt)^2 \right]^{\frac{1}{2}} \right\} \quad (25)$$

$$f(t) = -\left(\Delta E + e_{\lambda}^1 - e_{\mu}^0 \right) t + \frac{1}{v} \ln \left\{ \frac{vt}{b} + \left[1 + \left(\frac{vt}{b} \right)^2 \right]^{\frac{1}{2}} \right\} \quad (26)$$

In many applications it will probably be necessary to solve Eq. (23) numerically. However, in the present paper we will resort to an approximation that involves considerably less computation. We use the Magnus approximation,⁷ which involves setting the solution \underline{U} at $t \rightarrow +\infty$ to the exponential of a matrix. The result is

$$\underline{U} = \exp \left\{ -i \begin{bmatrix} 0 & \underline{Q} \\ \underline{Q}^\dagger & 0 \end{bmatrix} \right\} \quad (27)$$

where \underline{U} is a $2N \times 2N$ matrix. The matrix \underline{Q} and its transpose \underline{Q}^T are defined by

$$\begin{aligned} Q_{\mu\lambda} &= \int_{-\infty}^{\infty} A_{\mu\lambda}(t) dt \\ &= 2C_{\mu\lambda} \int_0^{\infty} w_{01}(t) \cos[f(t)] dt \end{aligned} \quad (28)$$

Because of the form of Eq. (27), unitarity is preserved. In the limit of weak coupling, one may expand the exponential of Eq. (27) and recover the standard result of first order time dependent perturbation theory. Note also that integral in Eq. (28) could be evaluated using the stationary phase approximation. The integrand is rapidly oscillating except near the time corresponding to the surface crossing, so that the formalism reflects the expected semiclassical result. In the present work, however, the integrals will be evaluated by numerical quadrature.

We will denote the elements of \underline{U} by $U_{\lambda\mu}^{ij}(b)$, where $0 \leq i, j \leq 1$ and $1 \leq \lambda, \mu \leq N$. The superscripts denote the $N \times N$ blocks, the subscripts the elements within each block. In this paper, we are primarily interested in $U_{\lambda\mu}^{10}(b)$, the block of transition amplitudes between an initial covalent channel and a final ionic channel. For this case, the total cross section from an initial vibrational state μ to a final state λ is given by

$$\sigma_{\lambda\mu} = 2\pi \int_0^{\infty} |U_{\lambda\mu}^{10}(b)|^2 b db \quad (29)$$

We may also define a cross section summed over final states:

$$\sigma(u) = \sum_{\lambda=1}^N \sigma_{\lambda\mu} \quad (30)$$

We now briefly discuss the determination of the S matrix from the matrix \underline{U} . Recall that the squared magnitude of each element of \underline{U} gives the probability of the corresponding state-to-state transition. That is, each element of \underline{U} must be multiplied by some phase factor in order to obtain \underline{S} . This phase factor is not necessary for the present applications [Eqs. (29) and (30)], but it would be needed for a differential cross section. We adopt the procedure⁹ of multiplying elements of \underline{U} by phase factors depending on η_0 and η_1 , which are the single channel phase shifts obtained for the potentials $V_0(R)$ and $V_1(R)$ respectively. [Note that η_1 is the phase shift in addition to the standard coulomb phase shift]. The result may be summarized by writing

$$\underline{S} = \underline{\Lambda} \underline{U} \underline{\Lambda} \quad (31)$$

where $\underline{\Lambda}$ is a $2N \times 2N$ matrix given by

$$\underline{\Lambda} = \exp \left\{ i \begin{bmatrix} \eta_0 \underline{1} & \underline{0} \\ \underline{0} & \eta_1 \underline{1} \end{bmatrix} \right\} \quad (32)$$

This formal prescription amounts to multiplying each element of the ij block of \underline{U} by $\exp [i(\eta_i + \eta_j)]$, for $i, j = 0, 1$.

2. Anisotropic Potentials

To include rotational degrees of freedom in the model it is necessary to include the anisotropy of the interaction potential. We generalize the potentials in the following way, according to the coordinates shown in Figure 1.

$$V_0(R, \gamma) = V(R_1) + V(R_2) \quad (33)$$

$$V_1(R, \gamma) = V(R, \gamma) + \Delta E - \frac{0.5}{R_1} - \frac{0.5}{R_2} \quad (34)$$

$$= V_0(R, \gamma) + \Delta E - \frac{1}{R} - \frac{a^2}{R^3} P_2(\cos \gamma) + \dots \quad (35)$$

$$W_{01}(R, \gamma) = c_1 e^{-c_2 R} \sin 2\gamma \quad (36)$$

The potential V is an effective two-body potential between the projectile and each atom of the (homonuclear) diatomic target, which is assumed to have an internuclear separation of $2a$. As in the isotropic case, an exponential, repulsive form of $V(R)$ could be chosen. However, for the particular form of Eqs. (33) and (34), the results to be presented here do not depend on V since it does not appear in the difference potential. This form of V_0 and V_1 has been used previously.^{5,6} The angular dependence of W_{01} is chosen to be the same used by Kleyn et al.⁸ for $\text{Cs} + \text{O}_2$, and has nodes at the angles required by symmetry.¹⁰

We now obtain rotationally-averaged cross sections using the Infinite-Order-Sudden (IOS) approximation,^{11,12} in which the cross section averaged

over initial rotational states and summed over final states is obtained by averaging the cross sections obtained in a set of calculations in which γ is regarded as a parameter. In other words, the rotationally averaged cross section $\sigma_{\lambda\mu}$ from an initial vibrational state μ to a final vibrational state λ is given by

$$\sigma_{\lambda\mu} = \frac{1}{2} \int_0^\pi \sigma_{\lambda\mu}(\gamma) \sin \gamma d\gamma \quad (37)$$

where $\sigma_{\lambda\mu}(\gamma)$ is the cross section obtained for "frozen" γ . When γ is fixed it is easy to calculate the cross sections for ion pair formation, using the methods of the preceeding section, for the form of V_0 and V_1 given in Eqs. (33) and (34). The result for $U(\gamma)$ is given by an equation of the same form as Eq. (27), with

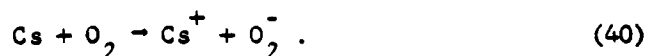
$$Q_{\mu\lambda}(\gamma) = 2C_{\mu\lambda} \sin 2\gamma \int_0^\infty \omega_{01}(t) \cos[f_\gamma(t)] dt \quad (38)$$

where

$$f_\gamma(t) = f(t) - \frac{a^2 P_2(\cos \gamma)}{vb^2} \left(\frac{vt}{b} \right) \left[1 + \left(\frac{vt}{b} \right)^2 \right]^{-\frac{1}{2}} \quad (39)$$

III. RESULTS AND DISCUSSION

The formalism developed in the preceeding section has been applied with parameters chosen to model the reaction



Initially we used an interaction potential without anisotropy. In a second calculation, however, anisotropy is included, and rotationally averaged cross sections are obtained using the IOS approximation. For both of the calculations we included 12 vibrational states of O_2 and 12 of O_2^- . This number was sufficient for convergence. The energy levels ϵ_u^0 and ϵ_v^1 and overlap integrals C_{uv} were calculated numerically using the Morse potentials for O_2 and O_2^- defined by Eq. (21) and Table 1. Other parameters for the potentials are also listed in Table 1.

The results of the first calculation are shown in Figure 2. Total cross sections for ion-pair formation are shown as a function of energy. The cross sections are summed over transitions from the indicated initial vibrational state to all final vibrational states. The most interesting feature is the pronounced oscillations. These have been previously interpreted^{2,6} in terms of a classical trajectory-hopping model, which is briefly summarized here. The basic idea is that the crossing point (or seam) of the covalent and ionic potential surfaces depends on the

vibrational coordinate. On the inward part of the trajectory, if the O_2 is in the $v=0$ state, the vibrational coordinate is localized near its equilibrium value, and the crossing occurs at $R \approx 7.2 a_0$. If a crossing to the ionic surface occurs, however, O_2^- will be formed, and the vibrational coordinate will start to expand, since the equilibrium separation of O_2^- is larger than that of O_2 . Depending on the relative translational velocity, the O_2^- may undergo a fraction of a vibration or several vibrations before the crossing seam is reached a second time. If the O_2^- is fully expanded at the second crossing, this crossing will occur at a larger value of R , and the matrix element for recrossing to the covalent surface will be much smaller, because of the exponential dependence of $W_{01}(R)$. In other words, if the O_2^- undergoes a half-integral number of vibrations between the surface crossings, the cross section for ion-pair formation will be enhanced.

This classical model has successfully explained the oscillations observed in the experimental data of Kleyn et al.⁸ It is worth noting, however, that except for a few exceptions,¹³ the previous calculations have assumed that the O_2^- begins at rest in the bottom of its potential well. Our present calculations show that the oscillations persist in a model that treats the diatomic target quantum mechanically. We are also able to examine the effect of changing the initial vibrational state of O_2 . It is seen that the oscillations tend to become less pronounced as

v_1 is increased. A possible explanation for this effect is that as v_1 increases, the spatial extent of the O_2 vibration increases, and it becomes more difficult to localize the first crossing. The oscillations depend on the first and second crossings occurring at very different values of R .

In Figure 3, we show the results of calculations in which an anisotropic term of the potential is treated using the IOS approximation. Compared to Figure 2, it is seen that the anisotropy causes the oscillations to be less pronounced, but that the same trends persist. Figure 4 compares the theoretical results for $v_1 = 0$ with the data of Kleyn et al. The trajectory hopping calculation of Kleyn et al.⁶ is also shown. All theoretical cross sections have been multiplied by a statistical factor of 1/3. Qualitative agreement between experiment and the present theory is obtained. It is likely that the position of the maximum in the theory could be brought into closer agreement with experiment by adjusting the parameters c_1 and c_2 of the coupling. We have simply taken the values obtained by Kleyn et al.⁶ by fitting their classical calculations to the data. (If the data of Kleyn et al. presented in Figure 4 are scaled by a constant factor, the agreement with the classical calculation is reasonable. This procedure is justified because the experimental cross sections are relative.)

A possible refinement to the theory, which would improve the threshold behavior, would be to include a factor $(E_f/E_i)^{1/2}$ in the cross section formulas. An empirical correction of this form has sometimes been used¹⁴ to insure that the cross section goes to zero at threshold. For energies near threshold, the assumption of a straight-line, constant velocity trajectory is not valid. We have not included this factor in the present calculations. For the cross sections at the lowest energies presented in Figures 2, 3, and 4, the correction would be on the order of 10%.

It is interesting to consider what might cause the difference between the surface-hopping calculation and the present model. Both use essentially the same potentials, yet the difference at some energies is as much as a factor of two. The discrepancy may be related to the following points. First, the rotation of the target is handled differently in the two models. In the present work, introducing the IOS approximation causes the location of the broad peak in the cross section to shift about 40% (cf. Figures 2 and 3). This significant change suggests the cross sections may be sensitive to the treatment of the molecular anisotropy. Second, the Magnus approximation may not provide a sufficiently accurate solution to Eq. (23). Finally, the Landau-Zener formula used in the classical model often underestimates transition probabilities at high energies.¹⁵ Further work is necessary before firm conclusions can be drawn.

IV. CONCLUDING REMARKS

We have presented the equations of the semiclassical impact parameter approximation for the case of collisions involving two potential surfaces, and have examined in detail their application to collisions of alkali atoms with diatomic molecules. Our results for the specific system $\text{Cs} + \text{O}_2$ are encouraging and suggest that the method may be of great value in fast collisions where successive curve crossings are not well isolated.

The present application has depended heavily on rather specific assumptions about the analytic form of the interaction potential. These assumptions were useful in order to simplify the numerical work required in the first application of the theory. However, a number of refinements may be introduced in a manner that is still computationally feasible. In particular, more general forms of the potentials $V_0(R)$ and $V_1(R)$ may easily be introduced. Including the non-separable terms, $W_{00}(R,r)$ and $W_{11}(R,r)$ is somewhat more difficult. Fortunately, experimental evidence⁸ seems to suggest that these terms may not be too important for collisions of alkali atoms and diatomic molecules.

Future work will focus on the applicability of the IOS to collisions involving two potential surfaces, and on the application of more refined numerical techniques for solving the equations of motion.

ACKNOWLEDGMENTS

This work was supported by the Air Force Office of Scientific Research. The author acknowledges helpful conversations with J. Pascale and R. P. Saxon.

REFERENCES

1. J. Los, in Proceedings of the Tenth International Conference on The Physics of Electronic and Atomic Collisions, Invited Papers and Progress Reports, ed. G. Watel (North Holland, Amsterdam, 1978.) p. 617.
2. J. Los and A. W. Kleyn in Alkali Halide Vapors, eds. P. Davidovits and D. L. McFadden (Academic Press, New York, 1979), p. 275.
3. S. Wexler and E. K. Parks Ann. Rev. Phys. Chem. 30, 179 (1979).
4. S. Geltman, Topics in Atomic Collision Theory (Academic Press, New York, 1969) p. 192.
5. C. Evers, Chem. Phys. 21, 355 (1977).
6. A. P. Hickman and K. T. Gillen, submitted to J. Chem. Phys.
7. P. Pechukas and J. C. Light, J. Chem. Phys. 44, 3897 (1966).
8. A. W. Kleyn, M. M. Hubers, and J. Los, Chem. Phys. 34, 55 (1978).
9. W. H. Miller and F. T. Smith, Phys. Rev. A. 17, 939 (1978).
10. E. A. Gislason and J. G. Sachs, J. Chem. Phys. 62, 2678 (1975).
11. D. Secrest, J. Chem. Phys. 62, 710 (1975).
12. G. A. Parker and R. T. Pack, J. Chem. Phys. 68, 1585 (1978).
13. E. A. Gislason, A. W. Kleyn, and J. Los, Chem. Phys. Lett. 67, 252 (1979).
14. J. Pascale and P. M. Stone, J. Chem. Phys. 65, 5122 (1976).
15. M. B. Faist and R. D. Levine, J. Chem. Phys. 64, 2953 (1976).

Table 1: Potential parameters. All quantities are given in atomic units.

A_0	Morse Parameters for O_2	0.1880
r_0	Morse Parameters for O_2	2.281
β_0	Morse Parameters for O_2^-	1.418
A_1	Morse Parameters for O_2^-	0.1503
r_1	Morse Parameters for O_2^-	2.534
β_1	Morse Parameters for O_2^-	1.090
$2a$	Internuclear separation of O_2	2.4
ΔE	Asymptotic energy separation	0.126
c_1	Defines coupling matrix element	0.35
c_2	Defines coupling matrix element	0.5

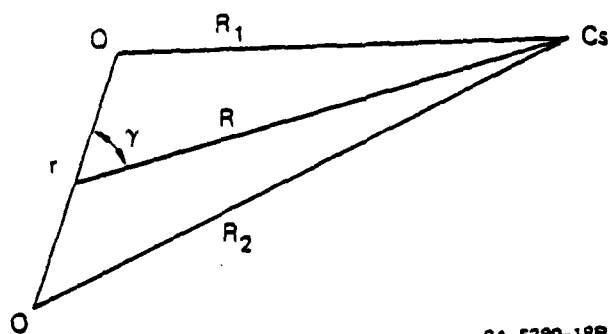
Figure Captions

Figure 1. Diagram illustrating the coordinates used on the present calculations.

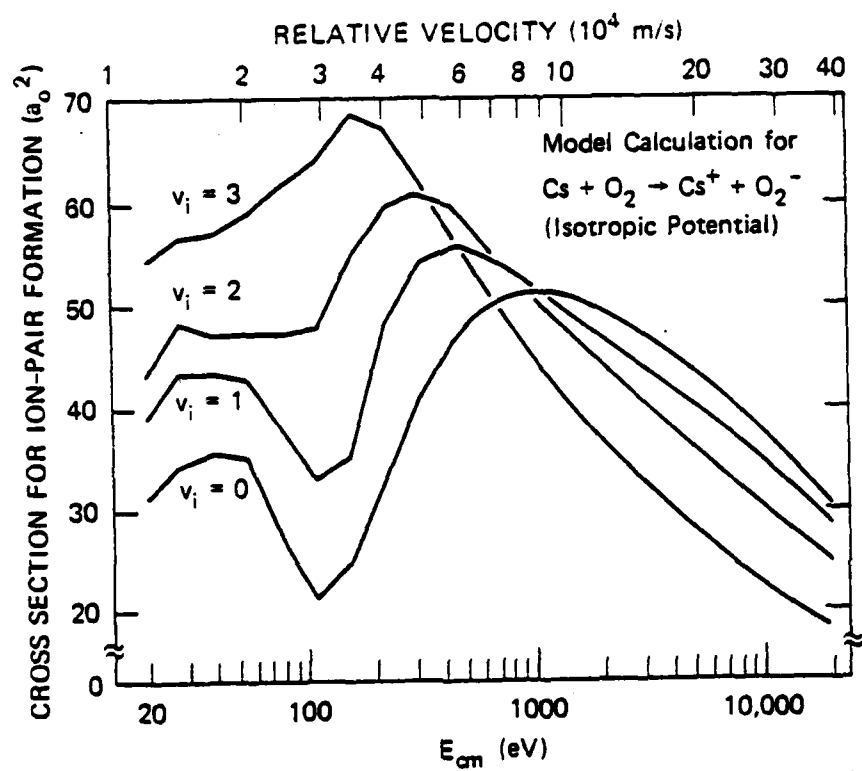
Figure 2. Results of the model calculation of the cross section for ion-pair formation in collisions of $\text{Cs} + \text{O}_2$. An isotropic potential is used as defined in Eqs. (17)-(21) and Table 1. The cross sections are summed over all (12) final vibrational states.

Figure 3. Results of the model calculation of the cross section for ion-pair formation in collisions of $\text{Cs} + \text{O}_2$. The anisotropic potential defined by Eqs. (33)-(36) is used, and the cross sections are summed over all (12) final vibrational states.

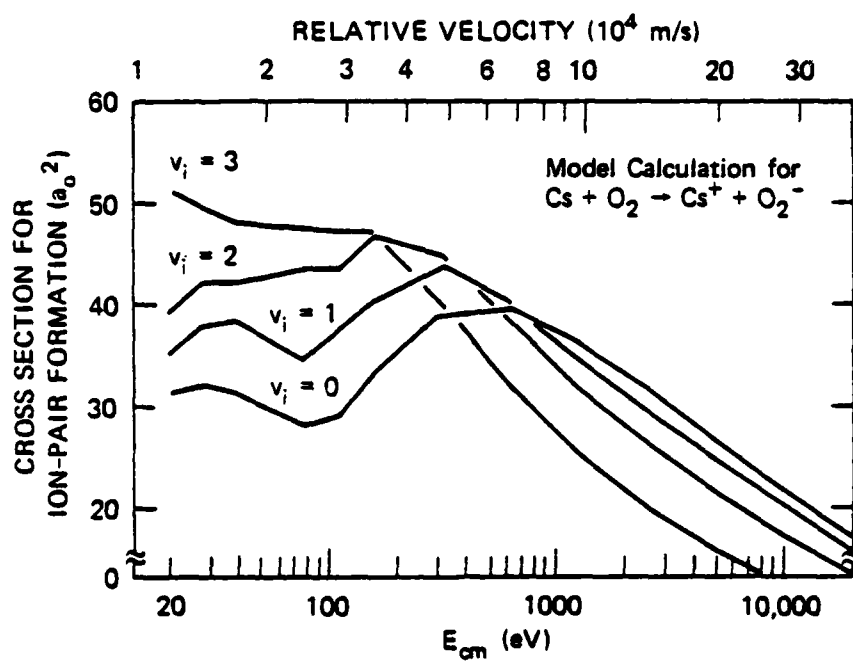
Figure 4. Comparison of the present model with the experimental results and calculations of Kleyn et al. The latter calculation was fitted to the data; if the experimental cross sections, which are relative, are scaled by a constant the agreement with that calculation is reasonable.



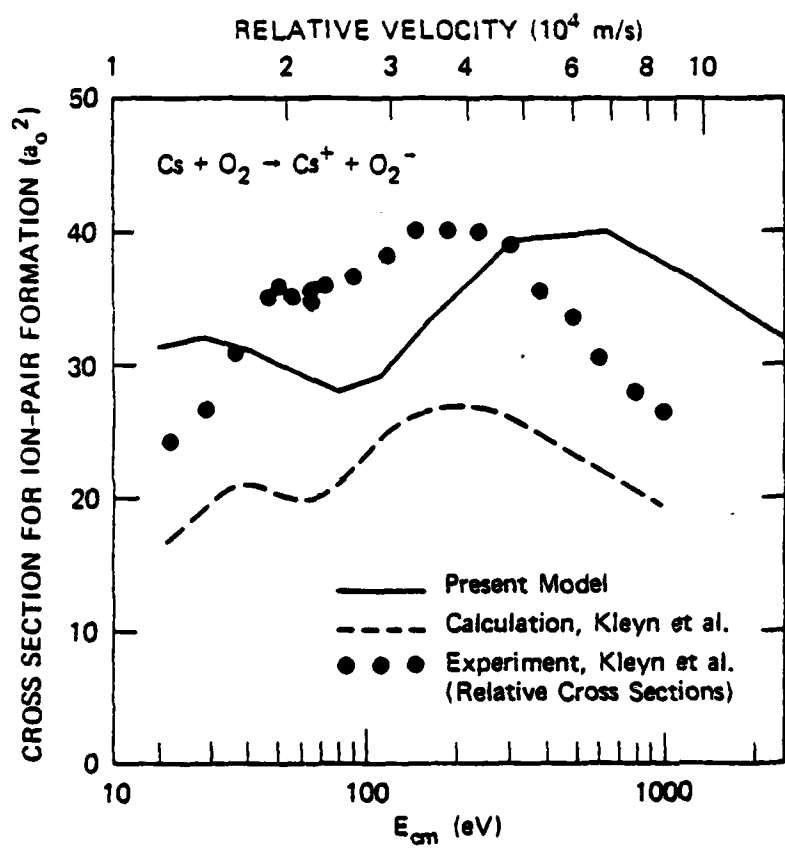
SA-5389-18R1



SA-4217-55



SA-4217-54



SA-4217-53